Angle-resolved photoemission studies of adsorbed hydrocarbons

1996 J. Phys.: Condens. Matter 8 6465

(http://iopscience.iop.org/0953-8984/8/36/003)

J. Phys.: Condens. Matter **8** (1996) 6465–6509. Printed in the UK

REVIEW ARTICLE

Angle-resolved photoemission studies of adsorbed hydrocarbons

Hans-Peter Steinrück

Experimentelle Physik II, Universität Würzburg, Am Hubland, D-97074 Würzburg, Germany

Received 20 March 1996, in final form 31 May 1996

Abstract. Angle-resolved UV photoelectron spectroscopy is used to investigate the electronic structure and bonding of adsorbed hydrocarbons, the orientation and symmetry of the adsorbate on the surface, the influence of lateral interactions, and the formation of two-dimensional adsorbate band structures. Several examples of simple hydrocarbon molecules such as benzene, ethylene and acetylene adsorbed on Ni(110), Ni(111), Ru(001) and the reconstructed Pt(110)1×2 surface are presented. The experimental studies are accompanied by theoretical calculations. In addition some special aspects of the photoemission process, namely the photoionization cross section and vibronic coupling, are discussed.

Contents

0953-8984/96/366465+45$19.50

1. Introduction

The adsorption of hydrocarbons, especially on metal surfaces, has aroused considerable interest from the very beginning of surface science. This interest originates in the central importance of these molecules in many catalytic processes and in technology. In particular small hydrocarbon molecules have been and are still considered not only to represent model systems for technologically relevant processes, but they are also interesting from the point of view of fundamental research. To investigate their vibrational, electronic and geometric properties, a variety of experimental techniques have been applied. These methods include high-resolution electron energy-loss spectroscopy (HREELS), temperature-programmed desorption (TPD), low-energy electron diffraction (LEED), near-edge x-ray absorption fine-structure (NEXAFS), scanning tunnelling microscopy (STM), x-ray photoelectron spectroscopy (XPS) and UV photoelectron spectroscopy (UPS) and several other techniques.

In this article, results obtained by angle-resolved UV photoelectron spectroscopy (ARUPS) for the smallest non-saturated hydrocarbon molecules acetylene and ethylene and for the aromatic benzene molecule adsorbed on transition metal surfaces will be reviewed, using examples mainly obtained in the author's group. The restriction to those molecules is motivated by several reasons.

(1) They represent model systems for the interaction of hydrocarbons with metal surfaces and they often serve as building blocks for larger organic molecules. The detailed knowledge of their adsorption characteristics is thus essential for the understanding of more complicated systems.

(2) The molecules are highly symmetric and in many cases adsorb in well defined adsorption geometries on the surface. This allows one to study the adsorbate/substrate interaction in great detail. In particular for adsorption on surfaces with twofold symmetry, such as the fcc(110) surfaces, far-reaching conclusions on the orientation of the molecules and the symmetry of the adsorption complex adsorbate + substrate can be derived.

(3) The most detailed understanding of the electronic structure and also the influence of lateral interactions in densely packed layers has been achieved for these adsorbate systems.

(4) They represent the only examples for hydrocarbon adsorbates where the formation of adsorbate band structures has been investigated.

(5) For some of the examples model cluster calculations, slab calculations, force-field calculations or tight-binding band-structure calculations are available that have helped in the obtaining of a deeper understanding.

All of the adsorbate systems that will be discussed below have been investigated not only via angle-resolved photoemission but also via a variety of other methods. In this article we will, however, concentrate on the results obtained by ARUPS and refer to other experimental results only if necessary. In the following we will briefly review some basics of angle-resolved photoemission in section 2 and provide some experimental aspects in section 3. Thereafter, the orientation and symmetry of adsorbed molecules will be discussed in section 4 with particular emphasis on the influence of lateral interactions. The electronic structure and bonding will be the subject of section 5. In section 6 we will address the formation of two-dimensional adsorbate band structures and in section 7 some special aspects, namely the photoionization cross section and vibronic coupling in the photoemission process of hydrocarbons, will be discussed.

2. Angle-resolved photoemission

ARUPS is an established technique in surface science [1–6] that is particularly well suited for studying the electronic structure of adsorbates on solid surfaces [7–17]. By investigating the outer valence region, modifications induced by the physical and/or chemical bond between adsorbate and substrate can be studied. From the comparison of the energetic positions of the electronic levels of the adsorbed species to the corresponding values for the free atom or molecule, direct and detailed information on the nature of the bond to the surface and on the chemical identity of the adsorbate can be deduced; the polarization and angular dependence of the emission from valence levels allows one to reach specific conclusions about the orientation of a molecule, and the symmetry of the adsorption complex. Furthermore, angle-resolved UV photoemission is the only technique for determining the band structures of adsorbate layers. The theoretical background of ARUPS has been discussed in many articles (see, e.g., references [1–17]). Here we will concentrate only on those aspects that will be of importance later on.

2.1. Energetic considerations

The electronic structure of a free or an adsorbed molecule is a more or less unique fingerprint of its chemical state. Therefore, one should—at least in principle—be able to identify the chemical identity of an adsorbed species from the ARUPS spectrum and decide whether a molecule adsorbs intact or decomposes during the adsorption process. From the binding energies of the individual electronic levels and in particular from the changes that occur upon adsorption, details of the electronic structure of the adsorbate and on the chemical bond between adsorbate and substrate can be derived.

As an example for the changes in the UPS spectra that are observed upon adsorption of a molecule on a surface, angle-integrated spectra of gaseous and chemisorbed benzene are compared in figure 1. The upper spectrum represents the spectrum of the free molecule with the energetic positions of the various valence levels and their assignment indicated. For several peaks the vibrational fine structure is well resolved. Upon adsorption significant changes occur, as is evident from the bottom of figure 1 where the UPS spectrum of benzene chemisorbed on Ni(111) is shown. The spectrum of the adsorbate layer contains the modified levels of the free molecule plus the emission from the substrate. The substrate-induced intensity is composed of direct emission of the substrate valence bands and secondary electrons due to inelastic scattering off the substrate or the adsorbate layer. The adsorbate levels are significantly broadened due to initial- and final-state effects, a common observation for adsorbed molecules [18–27]. The initial-state broadening is due to the coupling to the substrate bands [18]; the final-state effects include inelastic processes such as electron–hole pairs and phonon excitations, a reduced lifetime of the excitation due to the coupling to the substrate, and inhomogeneous screening of the ionic final state [19–26]. While binding energies for free molecules are referenced to the vacuum level, for adsorbed species they are usually given with respect to the Fermi level. The energetic difference between the Fermi level and the vacuum level is the work function Φ of the adsorbate layer. In comparison to the free molecule, the orbitals of the adsorbate undergo a more or less uniform relaxation shift, E_{Rel}, towards lower binding energies that is mainly attributed to extramolecular screening (a final-state effect) within the adsorbate layer and by the substrate [8, 20, 28]. For chemisorbed molecules, an additional differential shift of one or several molecular levels towards higher binding energies is observed. This shift reflects the participation of these levels in the chemical bond to the substrate (an initial-state effect)

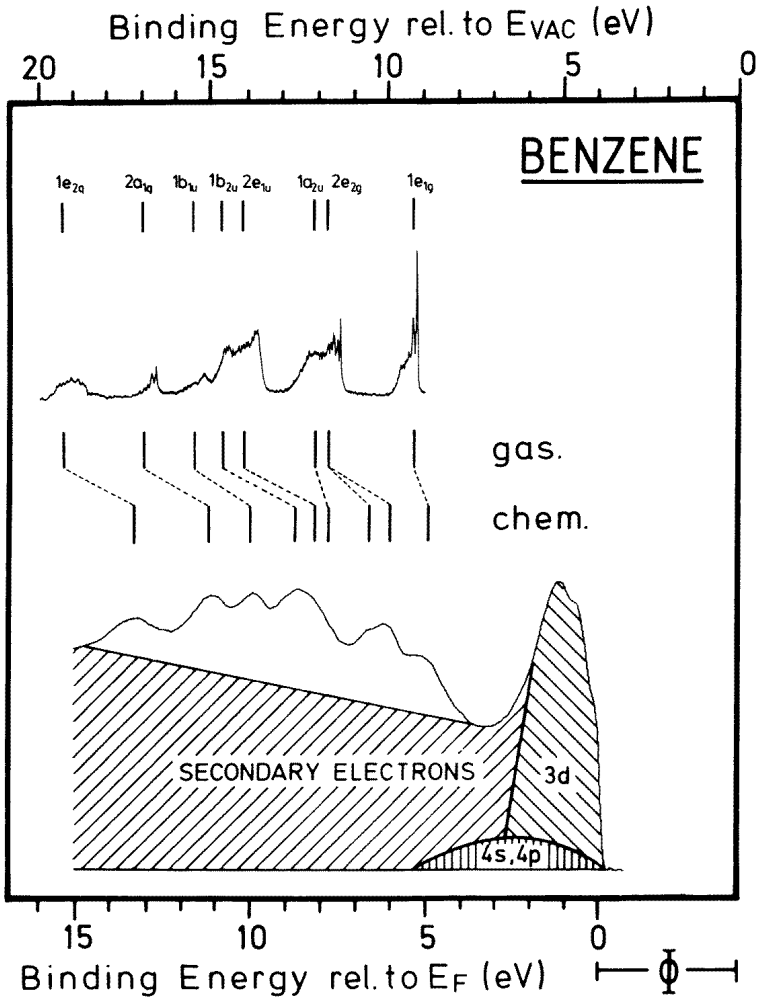

Figure 1. A schematic illustration of the changes in the photoelectron spectra that occur upon chemisorption [15]. Top: a UPS spectrum of gaseous benzene; bottom: a UPS spectrum of benzene chemisorbed on Ni(111). Φ: the work function of the adsorbate-covered surface.

and is referred to as the bonding shift E_{Bond} [8, 20, 27–30]. To a first approximation the binding energy of electrons in a particular adsorbate molecular level is then given by

$$E_B(\text{ad}) = E_B(\text{gas}) - E_{Rel} + E_{Bond} - \Phi. \tag{1}$$

The separation of relaxation shifts and bonding shifts is difficult. The common procedure for deducing the bonding shift is to assume identical relaxation shifts for those orbitals involved in the bond to the substrate and for those unaffected by this interaction. For benzene chemisorbed on metal surfaces the relaxation shift E_{Rel} is typically between 1.5 and 2.2 eV and bonding shifts E_{Bond} of 1.0–1.5 eV are observed for the two out-of-plane π-orbitals ($1a_{2u}$ and $1e_{1g}$) that are made responsible for the bonding interaction to the substrate.

The assumption of identical relaxation shifts for all orbitals should however be treated

with some caution. The change of the intramolecular bond length due to the chemisorptive bond can lead to differential shifts of molecular orbitals that are not primarily involved in the adsorbate substrate bond. This conclusion is supported by cluster calculations (see, e.g., references [30–32]) that reveal small energetic shifts ('chemical shifts') of those orbitals up to several tenths of one eV. Moreover, the comparison of the binding energies of particular levels of the adsorbate to those of the free molecule can be complicated by the formation of adsorbate band structures, i.e. a dependence of the binding energy on the momentum of the emitted electron. The corresponding band width can be as large as 2 eV for hydrocarbon molecules (see section 6), but has very often been neglected in the literature. For a meaningful comparison with the spectrum of the free molecule an adequate integration over the adsorbate surface Brillouin zone has to be performed.

2.2. Symmetry selection rules

The differential cross section for the photoemission process in the dipole approximation is given by Fermi's Golden Rule:

$$\mathrm{d}\sigma/\mathrm{d}\Omega \approx |\langle\Phi_f|\mu|\Phi_i\rangle|^2\delta(E_f - E_i - \hbar\omega). \tag{2}$$

In the single-particle approximation that has proven to be sufficient for most investigations on adsorbate layers [8], the initial state $|\Phi_i\rangle$ represents the bound electron in a particular orbital, the final state $\langle\Phi_f|$ the emitted electron, and $\mu = \boldsymbol{A}_0 \cdot \boldsymbol{p}$ the dipole operator. One major difference between free and adsorbed molecules is that the latter in many cases have a well defined orientation with respect to the substrate. Therefore, the differential cross section can be investigated in great detail by polarization-dependent ARUPS measurements: the final state is then uniquely specified by the kinetic energy E_{Kin} and the momentum $\boldsymbol{k}$ of the outgoing electron, as determined by an angle-resolving electron spectrometer; the initial state is given by the particular orbital of the oriented molecule; and the dipole operator μ is defined by the polarization of the incoming photon beam.

Calculations of the differential photoionization cross section for the various orbitals of adsorbates at selected photon energies are very complicated, if the surface and the changes induced by the chemical bond are properly taken into account [33–35]. For larger than diatomic adsorbates no such calculations are available. Nevertheless, detailed information on the orientation and symmetry of adsorbed molecules can be obtained from ARUPS data in combination with so-called symmetry selection rules [7, 8, 36, 37]. These rules are derived from the fact that in order to be non-zero, the dipole matrix element in equation (2)

$$M_{if} = \langle\Phi_f|\mu|\Phi_i\rangle \tag{3}$$

must be totally symmetric, or (for point groups with degenerate representations) at least contain a totally symmetric component [7, 8, 15, 36, 37]. The dipole operator μ transforms as the cartesian axes x, y, and z of the point group of the system. The representation of μ is thus defined by the cartesian components of the vector potential $\boldsymbol{A}$ (or, alternatively, the electric field vector $\boldsymbol{E}$) of the incoming radiation. For consistency with the nomenclature used in the examples discussed below, $\boldsymbol{E}$ will be used to denote the polarization of the incoming radiation in the following.

For a given polarization, $\boldsymbol{E}$, excitations from an initial state Φ_i are only allowed to final states Φ_f of particular symmetry [7, 8, 15, 36, 37]. Using group theory, it is easy to show that the symmetry of those final states (i.e. outgoing electrons) that fulfil the requirement $M_{if} \neq 0$ is given by the direct product of the representations of the initial state and the dipole operator:

$$\Phi_i \otimes \boldsymbol{E} = \Phi_f. \tag{4}$$

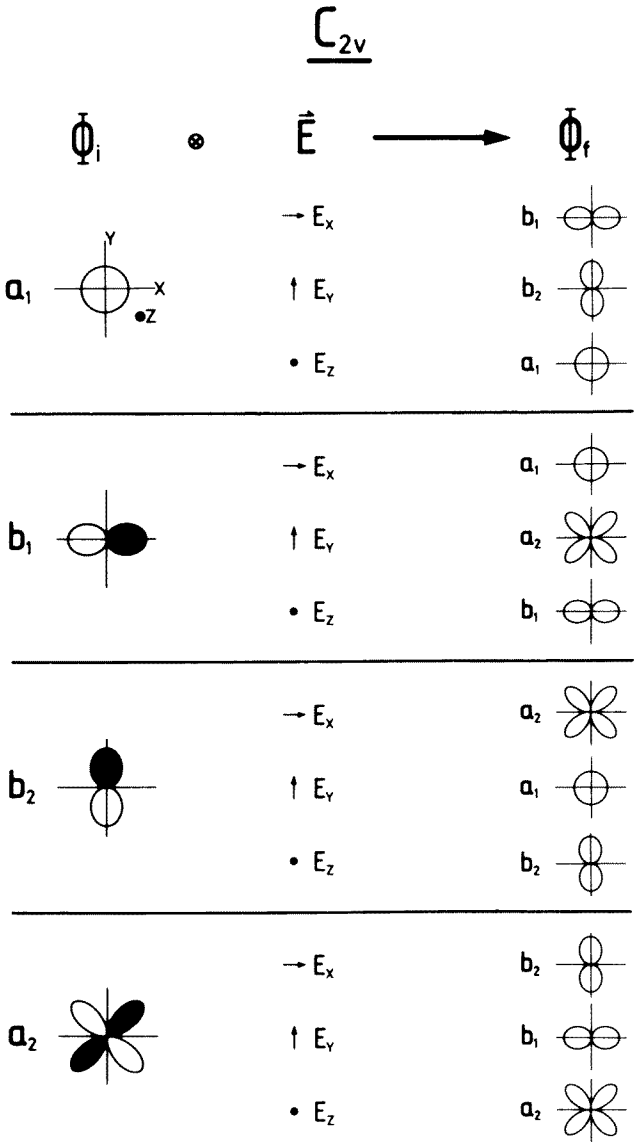

Figure 2. A schematic illustration of the predictions of symmetry selections rules for the point group C_{2v} [15]. The excitation from a particular initial state Φ_i (left) with a well defined polarization $\boldsymbol{E}$ (centre) leads to a specific final state Φ_f (right), according to equation (4). a_1 final states are allowed at any detector position; b_1 (b_2) final states are forbidden in normal emission and in the yz- (xz-) mirror plane (nodal planes of the final state) but are allowed in the xz- (yz-) mirror plane; a_2 final states are forbidden in normal emission and in both mirror planes.

Using symmetry selection rules, one can therefore predict whether emission from a specific orbital Φ_i is allowed or forbidden for a particular detector position and a given polarization. These rules are especially powerful if the detector is positioned in a high-symmetry direction, such as the surface normal or mirror planes of the system. In figure 2 a schematic illustration

of the predictions obtained by symmetry selection rules is given for the C_{2v} point group [15]. The excitation from a particular initial state Φ_i (left) with a well defined polarization $\boldsymbol{E}$ (centre) leads to a specific final state Φ_f (right), according to equation (4). For the final states very distinct emission characteristics are predicted: a_1 final states are allowed at any detector position; b_1 (b_2) final states are forbidden in normal emission and in the yz- (xz-) mirror plane (nodal planes of the final state) but are allowed in the xz- (yz-) mirror plane; a_2 final states are forbidden in normal emission and in both mirror planes.

The application of symmetry selection rules in many cases allows the assignment of peaks in the ARUPS spectra to orbitals or bands. Conversely, using a plausible peak assignment, symmetry selection rules allow one to obtain the orientation and symmetry of the adsorbate. One should note, however, that symmetry selection rules do not allow any predictions about the intensity of a particular final state: even if a final state is allowed by symmetry selection rules it can show vanishing intensity in the experiment due to cross sectional effects. This ambiguity can usually be overcome by making measurements at various photon energies.

2.3. Determination of adsorbate band structures

A well ordered adsorbate layer represents a two-dimensional superlattice on a surface with a two-dimensional periodic potential. If the intermolecular distances within the adsorbate lattice are small (roughly their Van der Waals dimensions), the overlap between neighbouring molecules is significant and the formation of a two-dimensional adsorbate band structure is expected [7, 8, 14–16, 28]. The adsorbate wave functions then have to be described as two-dimensional Bloch states $\Phi(\boldsymbol{k}_\parallel)$, with $\boldsymbol{k}_\parallel = \boldsymbol{k}_x + \boldsymbol{k}_y$, and the binding energy E_B depends on the electron momentum parallel to the surface $\boldsymbol{k}_\parallel$. The two-dimensional band structure $E_B(\boldsymbol{k}_\parallel)$ can be obtained from angle-resolved UPS spectra: the magnitude of the electron momentum parallel to the surface, $|\boldsymbol{k}_\parallel|$, is determined from the kinetic energy of the emitted photoelectron, E_{Kin}, and the polar angle of emission, ϑ, via the relationship

$$|\boldsymbol{k}_\parallel| = ((2m/\hbar^2)E_{Kin})^{1/2} \sin\vartheta \tag{5}$$

if one assumes a free-electron dispersion relation for the final state [8]. The two-dimensional band structure can then directly be plotted as the initial-state energy E_B versus $\boldsymbol{k}_\parallel$.

3. Experimental details

The angle-resolved UPS spectra have been collected at the Berlin Synchrotron facility BESSY using the TGM-1 monochromator [38]. The use of linearly polarized synchrotron radiation of high flux and tunable energy has turned out to be essential for obtaining detailed information about the electronic structure of adsorbates. It allows one to investigate effects related to the photoionization cross section and to measure adsorbate band structures up to large values of $k_\parallel$. The UHV system has been described elsewhere [39, 40]. The electron analyser is an angle–multichannel instrument developed at the Technische Universität München which allows simultaneous detection of electrons emitted under polar angles between $\vartheta = -10^\circ$ and 90° (with respect to the surface normal) at a given azimuth [41]. The analyser can be rotated around the surface normal of the crystal to put the detection plane D parallel or perpendicular to the plane defined by the electric field vector $\boldsymbol{E}$ of the incoming linearly polarized light and the surface normal. The simultaneous electron detection leads to a significant reduction of the collection time ($\sim$factor of 10) for an experimental data set as compared to that for conventional spectrometers, which is particularly important

for the determination of adsorbate band structures. Furthermore, the spectrometer permits measurements in normal emission ($\vartheta = 0^\circ$) at normal light incidence ($\alpha = 0^\circ$) which is very helpful for the determination of the adsorbate orientation in combination with symmetry selection rules.

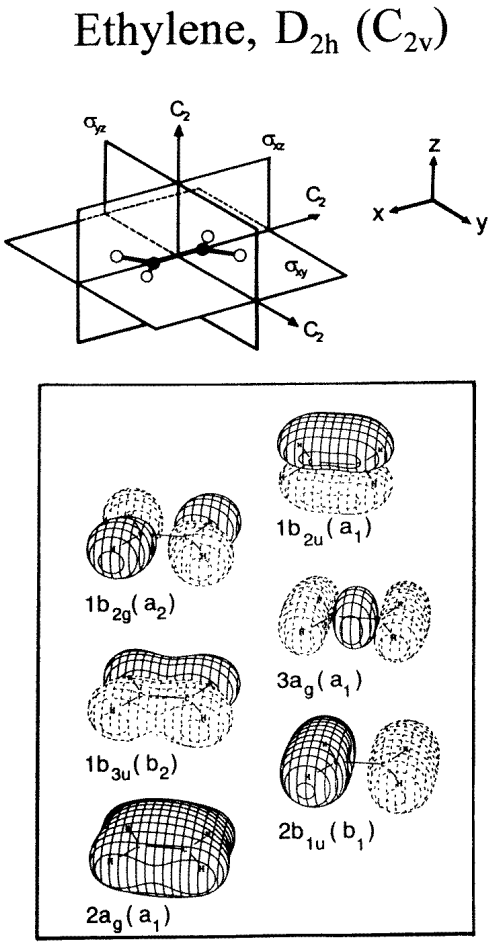

Figure 3. Top: a schematic drawing of ethylene with its symmetry elements; bottom: molecular orbitals of ethylene [31].

4. Orientation and symmetry of adsorbed molecules

A very important aspect of the bonding interaction of a molecule with a surface is the orientation of the molecule with respect to the substrate and the symmetry of the adsorption complex adsorbate + substrate. In many cases this symmetry will be lower than the symmetry of the free molecule: even in the case of a flat adsorption geometry of a planar molecule, the molecular plane is not a symmetry plane any more, due to the presence of the surface. For a single molecule on the surface, i.e. in the zero-coverage limit, the adsorbate/substrate interaction is determined by the electronic structure of both partners and

leads to a well defined adsorption geometry. For higher adsorbate coverages, the particular arrangement of the molecules is dictated by the interplay between adsorbate/substrate interaction and adsorbate/adsorbate interaction. Although in many cases the bonding to the substrate is significantly stronger than intermolecular interactions, the properties of densely packed adsorbate layers can be influenced very strongly by lateral (steric) interactions which can lead to changes in adsorption sites, bond lengths as well as orientation and symmetry with increasing coverage.

In order to obtain a detailed understanding of the adsorbate/substrate interaction, i.e. the 'vertical' interaction of a molecule with the surface, one would ideally investigate the properties of a single molecule on this substrate. This is however not possible due to the low intensity of the adsorbate-derived levels. To keep the influence of neighbouring molecules small, the experiments are performed for dilute adsorbate layers. Typical coverages in our studies range from 20 to 50% of the saturated chemisorbed layer. Measurements at even lower coverages are very difficult due to the low signal-to-noise ratio. To verify that lateral interactions are negligible or at least only very small, it has to be checked (e.g. by LEED) that no island formation occurs and/or that no adsorbate band structure is formed (by ARUPS). The measurements on dilute layers then can serve as the starting point for quantum chemical cluster calculations that provide more insight into the nature of the adsorbate/substrate interaction.

To investigate the influence of adsorbate/adsorbate interactions, measurements are in most cases performed for well ordered saturated layers which guarantee significant lateral interactions on the one hand and a well defined arrangement of the neighbouring atoms on the other hand. The experimental studies are supported by force-field calculations that allow one to determine the repulsive energy per molecule in a densely packed layer and to find the minimum-energy geometry. Despite the fact that these calculations are often performed for unsupported layers, they nevertheless have been shown to be very helpful for the simulation of adsorbate structures.

In the following the results for ethylene on Ni(110) and for pure and coadsorbed benzene layers on Ni(110) and Ni(111) and on Pt(110)1×2 will be reviewed. The main objective of the investigations on nickel was to determine the orientation and symmetry of the 'isolated' molecule on the surface which is governed by adsorbate/substrate interaction, and to search for the changes that are induced by lateral interactions in densely packed layers. The study on Pt(110)1×2 was performed to determine the adsorption geometry of benzene on a strongly corrugated surface.

4.1. Ethylene/Ni(110)

Ethylene (C_2H_4) is a non-saturated hydrocarbon molecule that is well known to chemisorb on transition metal surfaces (see, e.g., references [31, 42–51]). The majority of studies have been performed using HREELS to investigate its vibrational properties [47]. Information on the electronic structure is rather limited and, with very few exceptions [43–46], restricted to angle-integrated measurements at high coverages. The symmetry of the free ethylene molecule is D_{2h}; a schematic drawing of the molecule with its symmetry elements along with an overview of the spatial extension of the ethylene valence orbitals is shown in figure 3 [31]. Upon adsorption the highest possible symmetry is C_{2v}, due to the substrate–molecule–vacuum asymmetry. The particular interaction with the substrate can lower the symmetry even further: for C_2 symmetry the only remaining symmetry element is a twofold rotation axis C_2, and for $C_s(\sigma_{xz})$ or $C_s(\sigma_{yz})$ symmetry the remaining symmetry elements are the σ_{xz}- or the σ_{yz}-mirror planes, respectively. This lowering in symmetry leads to modified

Table 1. Symmetry selection rules for several molecular symmetries of ethylene for various experimental geometries. E_x, E_y and E_z denote the cartesian components of the electric field vector of the incoming light with respect to the surface plane and a flat-lying ethylene molecule (see figure 3 (top)); D_x and D_y characterize the alignment of the detection plane. 'N' indicates that a band is allowed in normal emission ($\vartheta = 0^\circ$) and at all other angles; '+' and '−' indicate that emission in the detection plane ($\vartheta \neq 0^\circ$) is allowed or forbidden, respectively.

D_{2h}	C_{2v}						
		E_xD_x	E_yD_y	E_xD_y	E_yD_x	E_zD_x	E_zD_y
b_{2u}, a_g	a_1	+	+	−	−	N	N
b_{2g}	a_2	−	−	+	+	−	−
b_{1u}	b_1	N	−	N	−	+	−
b_{3u}	b_2	−	N	−	N	−	+
D_{2h}	C_2						
		E_xD_x	E_yD_y	E_xD_y	E_yD_x	E_zD_x	E_zD_y
b_{2u}, a_g	a	+	+	+	+	N	N
b_{2g}	a	+	+	+	+	N	N
b_{1u}	b	N	N	N	N	+	+
b_{3u}	b	N	N	N	N	+	+
D_{6h}	$C_s(\sigma_{xz})$						
		E_xD_x	E_yD_y	E_xD_y	E_yD_x	E_zD_x	E_zD_y
b_{2u}, a_g	a′	N	+	N	−	N	N
b_{2g}	a″	−	N	+	N	−	+
b_{1u}	a′	N	+	N	−	N	N
b_{3u}	a″	−	N	+	N	−	+
D_{6h}	$C_s(\sigma_{yz})$						
		E_xD_x	E_yD_y	E_xD_y	E_yD_x	E_zD_x	E_zD_y
b_{2u}, a_g	a′	+	N	−	N	N	N
b_{2g}	a″	N	−	N	+	+	−
b_{1u}	a″	N	−	N	+	+	−
b_{3u}	a′	+	N	−	N	N	N

(relaxed) symmetry selection rules, as is illustrated in table 1, where the correlations between molecular orbitals for various possible point groups are summarized along with the corresponding symmetry selection rules.

4.1.1. The dilute ethylene layer. To investigate the adsorbate/substrate interaction, ARUPS measurements have been performed for a dilute ethylene layer that has been prepared by dosing 0.8 L ethylene onto the Ni(110) surface at temperatures below 120 K [31, 48]. It corresponds to a coverage of 0.25 ML (1 ML = 1 adsorbate molecule/substrate atom) which is one half of the saturation coverage. A selection of ARUPS spectra are depicted in figure 4. The spectra have been collected in various experimental geometries, with the electric field vector $\boldsymbol{E}$ aligned parallel to the closed-packed substrate rows (the $[1\bar{1}0]$ azimuth) or perpendicular to them (the [001] azimuth), and the plane of detection D parallel to $\boldsymbol{E}$ (D$\|\boldsymbol{E}$, allowed geometry). For normal incidence ($\alpha = 0^\circ$, only x- or y-components of $\boldsymbol{E}$), spectra are shown for emission angles ϑ of 0° (normal emission), 30°, and 60°; for $\alpha = 45^\circ$

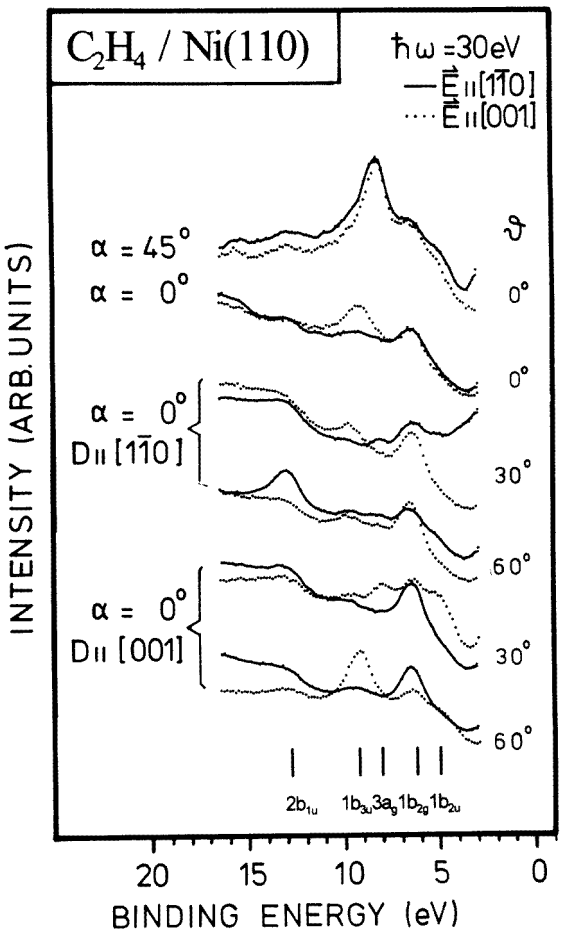

Figure 4. Angle-resolved UPS spectra of the dilute ethylene layer ($\theta = 0.25$ ML) on Ni(110) at different geometries, collected at a photon energy of 30 eV [31, 48]. The orbital positions and assignment are denoted as a bar diagram. D indicates the plane of detection, $\boldsymbol{E}$ the orientation of the electric field vector. α and ϑ are the photon angle of incidence and the electron emission angle, with respect to the surface normal, respectively.

($x + z$- or $y + z$-components of $\boldsymbol{E}$) spectra for $\vartheta = 0^\circ$ are shown. The comparison of the energetic position of the various levels with the corresponding values for the free molecule [52] reveals a bonding shift of 1.1 eV of the π-orbital ($1b_{2u}$) to higher binding energy due to the chemisorptive bond to the substrate. From the fact that the binding energies of the various molecular levels are independent of the azimuth and polar angle of emission within ± 0.1 eV (figure 5(a)) we conclude that lateral interactions are indeed not important and that the results discussed in this section are representative of the interaction of the single molecule with the Ni(110) surface.

The orientation and symmetry of ethylene on Ni(110) is determined from the distinct polarization, azimuthal and polar angle dependencies of the valence levels and symmetry selection rules [31, 48]: the parallel orientation of the molecule with respect to the surface is deduced from the behaviour of the $3a_g$ and $1b_{2u}$ orbitals at normal emission ($\vartheta = 0^\circ$). Both

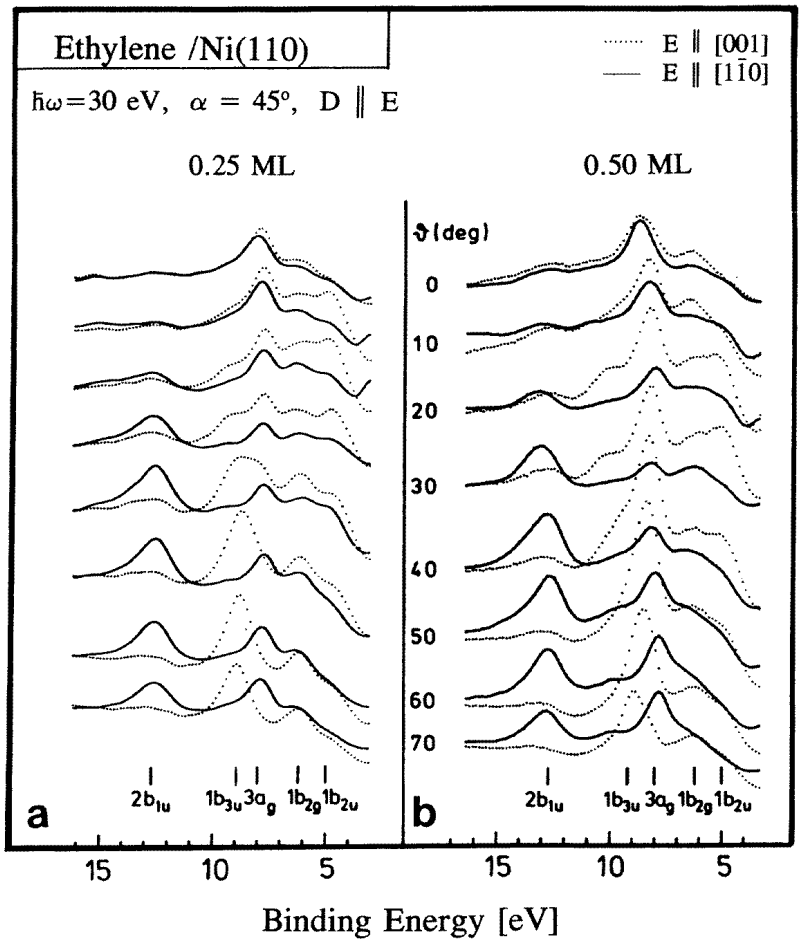

Figure 5. Angle-resolved UPS spectra of ethylene on Ni(110) for increasing polar angles ϑ at an incidence angle of $\alpha = 45^\circ$ and a photon energy of 30 eV. (a) The dilute layer, $\theta = 0.25$ ML [31]; (b) the saturated c(2 × 4) layer, $\theta = 0.50$ ML [49].

show significant intensity for $\alpha = 45^\circ$, but have vanished for $\alpha = 0^\circ$, i.e. for a zero E_z-component of the incoming radiation. Since both orbitals belong to the totally symmetric a_1 (a) representation for C_{2v} (C_2) symmetry, an orientation of the C–C axis parallel to the surface immediately follows. In addition, both orbitals show only weak emission (not shown [31]) in the so-called 'forbidden' geometry (D⊥ $\boldsymbol{E}$) indicating that the molecule is azimuthally well oriented. More information on the azimuthal orientation is derived from the behaviour of the $1b_{3u}$ and $2b_{1u}$ orbitals which belong to the b_2 and b_1 representations, respectively, if we assume a flat-lying ethylene molecule with C_{2v} symmetry. The $1b_{3u}$ orbital shows strong emission for $\boldsymbol{E}\|[001]$ and weak emission for $\boldsymbol{E}\|[1\bar{1}0]$; the $2b_{1u}$ orbital shows the opposite behaviour. By comparison to the predictions from symmetry selection rules for C_{2v} symmetry (see table 1) we conclude that the C–C axis is preferentially aligned with the densely packed substrate rows, i.e. the $[1\bar{1}0]$ azimuth. While the behaviour of the $1b_{2u}$, $3a_g$, $1b_{3u}$ and $2b_{1u}$ orbitals is consistent with C_{2v} symmetry, the non-zero normal emission ($\vartheta = 0^\circ$) from the $1b_{2g}$ orbital (a_2 in C_{2v}) in all geometries suggests that the

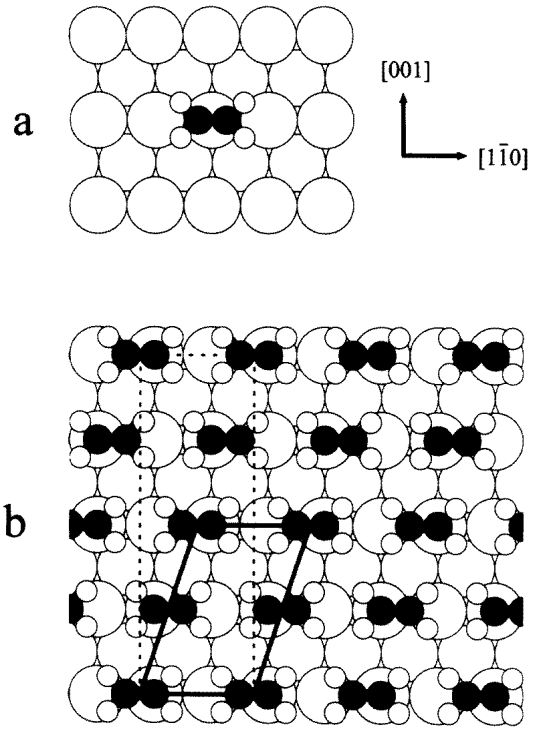

Figure 6. (a) A schematic drawing of the proposed orientation of a single ethylene molecule in the dilute layer on Ni(110) [31], with C_{2v} symmetry. Note that the adsorption site has been chosen arbitrarily. (b) A structural model for the densely packed c(2×4) ethylene layer on Ni(110) as determined from LEED, ARUPS and NEXAFS and force-field calculations [49].

symmetry of the adsorption complex is only C_1, probably due to a low-symmetry adsorption site and/or a twisting of the adsorbed molecule. A schematic drawing of the adsorption geometry (with C_{2v} symmetry) of ethylene on Ni(110) is given in figure 6(a).

4.1.2. The saturated c(2×4*) ethylene layer.* The saturated ethylene layer is well ordered and exhibits a c(2×4) LEED pattern with the $(0, \pm(1/2)(2n+1))$-order spots missing for normal incidence [49, 50]. The saturation coverage is 0.5 ML, indicating a non-primitive unit cell containing two ethylene molecules. The ARUPS spectra of the saturated layer (figure 5(b)) show essentially the same emission characteristics as those of the dilute layer (figure 5(a)), which indicates a coverage-independent orientation [49]. The major difference from the dilute layer is the significant dispersion (up to 2 eV) of various levels for the saturated layer that indicates the formation of a two-dimensional band structure (see section 6.2). From the c(2×4) structure and the well defined azimuthal orientation with the C–C axis aligned with the substrate rows, we deduce a compressed real-space structure as drawn in figure 6(b): the molecules are adsorbed in dense rows along the [1$\bar{1}$0] direction with every second substrate site being occupied. Neighbouring adsorbate rows are shifted relative to each other by half of a lattice vector along [1$\bar{1}$0]; the two molecules in the unit cell are related by a C_2 point transformation [49]. As a consequence (translationally) equivalent adsorption sites are occupied only every second row entailing a non-primitive oblique unit

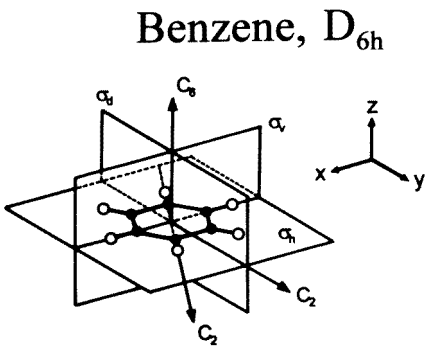

Figure 7. This page: a schematic drawing of benzene with its symmetry elements. Note that only one out of three equivalent C_2 rotation axes, σ_d- and σ_v-mirror planes are indicated. Facing page: molecular orbitals of benzene after Jorgensen and Salem [75].

cell for the c(2 × 4) structure. This structural model is confirmed by NEXAFS measurements and by force-field calculations [49].

4.2. Benzene/Ni(110)

The adsorption of benzene has been subject to numerous investigations in the past [13, 14, 39, 40, 47, 51, 53–74]. Like ethylene, benzene is a non-saturated hydrocarbon with a reactive π-system and therefore chemisorbs on transition metal surfaces. Most of the available information with respect to the electronic structure concerns saturated layers, and with few exceptions [72] a flat adsorption geometry is reported. Information on the azimuthal orientation and the influence of lateral interactions is however limited. The free benzene molecule is highly symmetric and belongs to the D_{6h} point group. A schematic drawing of the molecule and an overview of the spatial extension of its molecular orbitals is given in figure 7 [75]. Upon adsorption on a surface the highest possible symmetry is C_{6v}. This symmetry can be further lowered due to the particular interaction with the substrate. The correlations between possible point groups are summarized in table 2 along with the corresponding symmetry selection rules.

4.2.1. The dilute benzene layer. A selected set of ARUPS spectra for the dilute benzene layer on Ni(110) is depicted in figure 8(a) [63, 64]. This dilute layer has been prepared by exposing the surface to 0.7 L C_6D_6 [76] at 110 K; the corresponding coverage is 0.10 ML, which is 40% of the saturation coverage. The comparison of the energetic positions of the molecular levels in figure 8(a) to those of the free molecule [52] reveals differential shifts of the π-orbitals ($1a_{2u}$, $1e_{1g}$) by ∼1.1 eV towards higher binding energies which are attributed to the chemisorptive bond to the substrate. The molecular levels show significant dependencies on polarization and emission angle, but no dispersion within ±0.1 eV which indicates that lateral interactions are not important. From the ARUPS spectra, we conclude that benzene is oriented with its molecular plane parallel to the surface and two of the C–H bonds aligned along the [001] azimuths [63, 64]; the proposed arrangement is schematically shown in figure 9(a). The parallel orientation follows from the vanishing normal emission ($\vartheta = 0^\circ$) of the totally symmetric $2a_{1g}$ and $1a_{2u}$ levels for $\alpha = 0^\circ$ (normal incidence, only E_x or E_y) as compared to the very strong normal emission for $\alpha = 45^\circ$ ($E_z \neq 0$). The azimuthal alignment is deduced from the emission characteristics of the b-type orbitals for

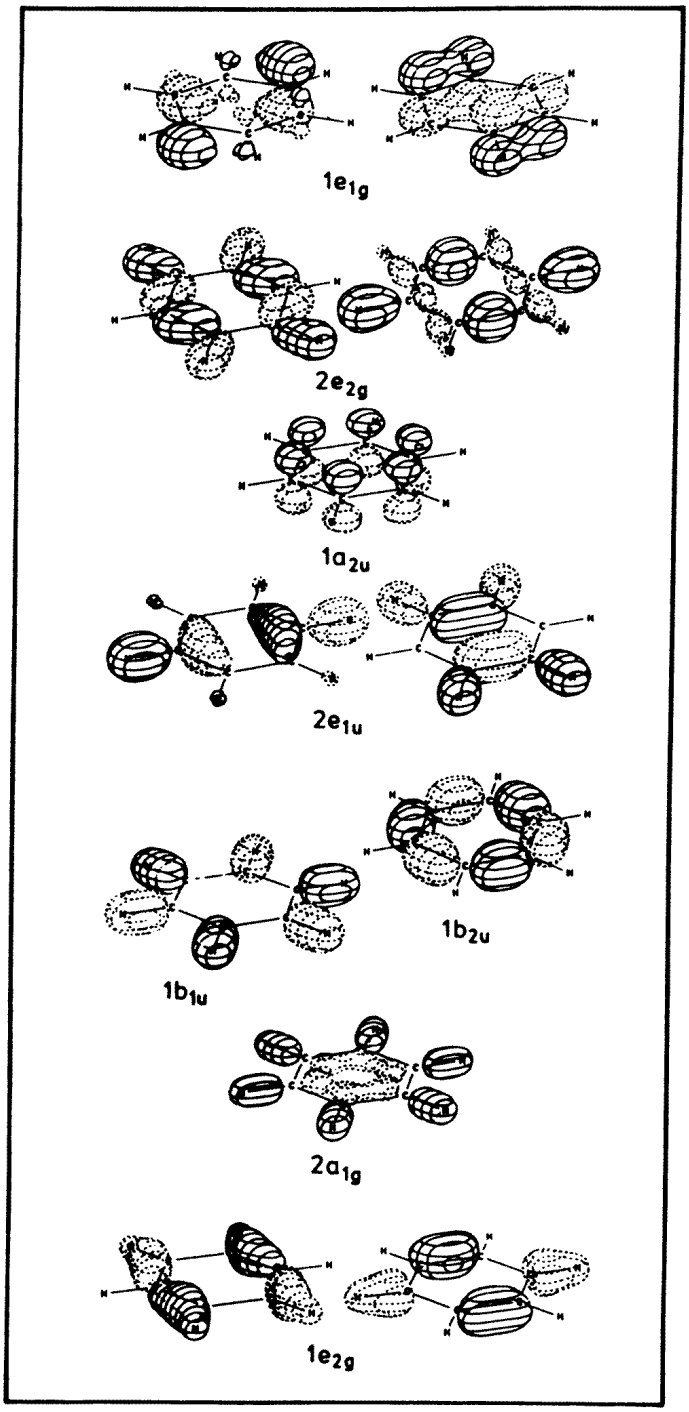

Figure 7. (Continued)

Table 2. Symmetry selection rules for several molecular symmetries of benzene for various experimental geometries. E_x, E_y and E_z denote the cartesian components of the electric field vector of the incoming light with respect to the surface plane and a flat-lying benzene molecule (see figure 7 (left)); D_x and D_y characterize the alignment of the detection plane. 'N' indicates that a band is allowed in normal emission ($\vartheta = 0°$) and at all other angles; '+' and '−' indicate that emission in the detection plane ($\vartheta \neq 0°$) is allowed or forbidden, respectively.

D_{6h}	C_{6v}						
		$E_x D_x$	$E_y D_y$	$E_x D_y$	$E_y D_x$	$E_z D_x$	$E_z D_y$
e_{1g}, e_{1u}	e_1	N	N	N	N	+	+
e_{2g}, e_{2u}	e_2	+	+	+	+	+	+
a_{1g}, a_{2u}	a_1	+	+	−	−	N	N
a_{2g}, a_{1u}	a_2	−	−	+	+	−	−
b_{1u}	b_1	+	−	+	−	+	−
b_{2u}	b_2	−	+	−	+	−	+
D_{6h}	$C_{3v}(\sigma_v)$						
		$E_x D_x$	$E_y D_y$	$E_x D_y$	$E_y D_x$	$E_z D_x$	$E_z D_y$
e_{1g}, e_{1u}	e	N	N	N	N	+	+
e_{2g}, e_{2u}	e	N	N	N	N	+	+
a_{1g}, a_{2u}	a_1	+	+	+	−	N	N
a_{2g}, a_{1u}	a_2	−	+	+	+	−	−
b_{1u}	a_1	+	+	+	−	N	N
b_{2u}	a_2	−	+	+	+	−	−
D_{6h}	C_{2v}						
		$E_x D_x$	$E_y D_y$	$E_x D_y$	$E_y D_x$	$E_z D_x$	$E_z D_y$
e_{1g}, e_{1u}	b_1	N	−	N	−	+	−
	b_2	−	N	−	N	−	+
e_{2g}, e_{2u}	a_1	+	+	−	−	N	N
	a_2	−	−	+	+	−	−
a_{1g}, a_{2u}	a_1	+	+	−	−	N	N
a_{2g}, a_{1u}	a_2	−	−	+	+	−	−
b_{1u}	b_1	N	−	N	−	+	−
b_{2u}	b_2	−	N	−	N	−	+
D_{6h}	C_2						
		$E_x D_x$	$E_y D_y$	$E_x D_y$	$E_y D_x$	$E_z D_x$	$E_z D_y$
e_{1g}, e_{1u}	b	N	N	N	N	+	+
	b	N	N	N	N	+	+
e_{2g}, e_{2u}	a	+	+	+	+	N	N
	a	+	+	+	+	N	N
a_{1g}, a_{2u}	a	+	+	+	+	N	N
a_{2g}, a_{1u}	a	+	+	+	+	N	N
b_{1u}	b	N	N	N	N	+	+
b_{2u}	b	N	N	N	N	+	+

$\alpha = 45°$: the $1b_{1u}$ orbital shows strong emission for $\boldsymbol{E}\|[001]$, but vanishes for $\boldsymbol{E}\|[1\bar{1}0]$; the $1b_{2u}$ orbital exhibits the opposite behaviour, namely strong emission for $\boldsymbol{E}\|[1\bar{1}0]$ and no emission for $\boldsymbol{E}\|[001]$. This behaviour indicates that the σ_v- and σ_d-mirror planes of the molecules coincide with the [001] and $[1\bar{1}0]$ substrate azimuths, respectively. Inspection

Table 2. (Continued)

D_{6h}	$C_s(\sigma_v)$						
		E_xD_x	E_yD_y	E_xD_y	E_yD_x	E_zD_x	E_zD_y
e_{1g}, e_{1u}	a′	N	+	N	−	N	N
	a″	−	N	+	N	−	+
e_{2g}, e_{2u}	a′	N	+	N	−	N	N
	a″	−	N	+	N	−	+
a_{1g}, a_{2u}	a′	N	+	N	−	N	N
a_{2g}, a_{1u}	a″	−	N	+	N	−	+
b_{1u}	a′	N	+	N	−	N	N
b_{2u}	a″	−	N	+	N	−	+
D_{6h}	$C_s(\sigma_d)$						
		E_xD_x	E_yD_y	E_xD_y	E_yD_x	E_zD_x	E_zD_y
e_{1g}, e_{1u}	a′	+	N	−	N	N	N
	a″	N	−	N	+	+	−
e_{2g}, e_{2u}	a′	+	N	−	N	N	N
	a″	N	−	N	+	+	−
a_{1g}, a_{2u}	a′	+	N	−	N	N	N
a_{2g}, a_{1u}	a″	N	−	N	+	+	−
b_{1u}	a″	N	−	N	+	+	−
b_{2u}	a′	+	N	−	N	N	N

of the e-type orbitals reveals a splitting of the $2e_{1u}$ level by 0.3 eV (which is particularly evident at normal emission for $\alpha = 0^\circ$) and of the $1e_{1g}$ level by 0.2 eV; this indicates a lifting of the degeneracy of these levels for the adsorbed molecules and C_{2v} symmetry of the adsorption complex [63]. The double-peak structure of the $2e_{2g}$ level has a different origin, namely the Jahn–Teller effect, as will be discussed in section 7.2.

4.2.2. The saturated c(4 × 2) benzene layer. To investigate the influence of lateral interactions, the benzene coverage is increased to its saturation value, namely $\theta_{SAT} = 0.25$ ML. This layer is well ordered and exhibits a c(4 × 2) LEED pattern [63, 64]. The arrangement of the molecules in this structure is again deduced from the polarization, polar angle and azimuthal dependencies of the corresponding ARUPS spectra that are depicted in figure 8(b): the totally symmetric $2a_{1g}$ and $1a_{2u}$ orbitals show the same behaviour as for the dilute layer, i.e. strong normal emission for $\alpha = 45^\circ$ and no emission for $\alpha = 0^\circ$, indicating a planar adsorption geometry. However, in contrast to the dilute layer, both the $1b_{1u}$ orbital and the $1b_{2u}$ orbitals are observed for the $[1\bar{1}0]$ and [001] azimuth at $\alpha = 45^\circ$ in figure 8(b). From this behaviour we conclude that in the saturated layer the molecular mirror planes do not coincide with the substrate mirror planes any more. This lowering in symmetry is attributed to an azimuthal reorientation (rotation) of the benzene molecules [63] due to strong lateral interactions in the densely packed saturated layer. The proposed arrangement of the molecules on the surface is schematically illustrated in figure 9(b).

In order to obtain a better understanding of the mechanism that drives the reorientation of the molecules, the c(4 × 2) structure is shown in figure 10 (top, I–III) for various possible azimuthal orientations of the benzene molecules; the sizes of the molecules represent their Van der Waals dimensions. Due to the dense packing, there is a significant overlap of the Van der Waals areas of neighbouring molecules. This overlap is strongest for an azimuthal

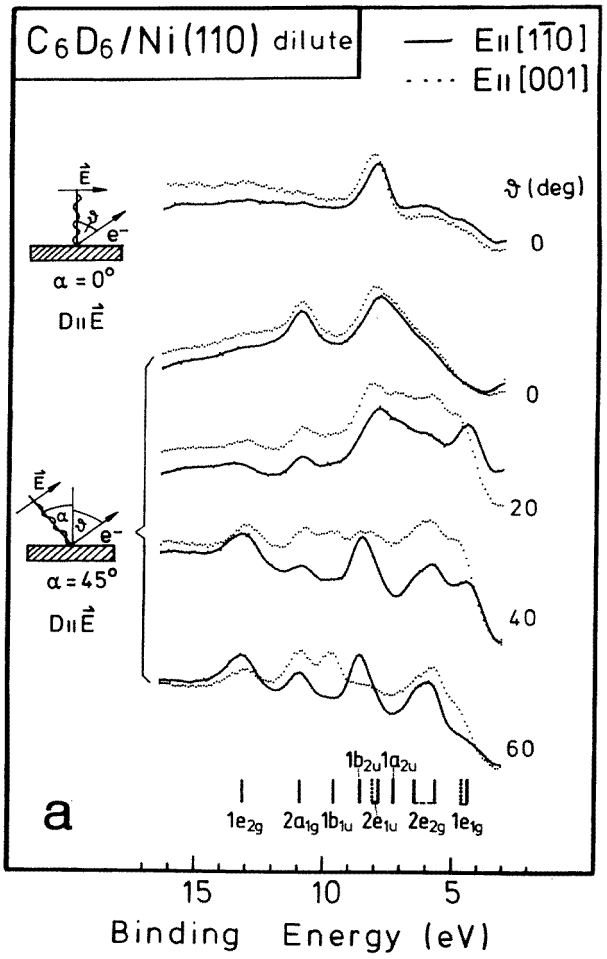

Figure 8. Angle-resolved UPS spectra of benzene on Ni(110) at various different geometries, collected at a photon energy of 30 eV [63]. (a) The dilute layer (θ = 0.1 ML = $0.4\theta_{SAT}$) and (b) the saturated c(4 × 2) layer (θ = 0.25 ML). Orbital positions and the assignment are indicated as a bar diagram.

orientation as for the isolated molecule (figure 10, I), i.e. with two C–H bonds pointing along the [001] directions. By azimuthal rotation relative to the geometry of the isolated molecule (figures 10, II and 10, III), the overlap can be reduced to minimize lateral repulsion and thereby to lower the total energy of the system. These qualitative arguments are put onto a more quantitative footing by force-field calculations by Fox and Rösch [77]. They have calculated the repulsive energy per molecule as a function of the rotation angle, ϕ, for an unsupported benzene layer (figure 10, bottom). In agreement with the intuitive arguments used above, this calculation shows a very large repulsive energy for $\phi = 0^\circ$ which corresponds to the orientation of the isolated molecule. Upon azimuthal rotation the repulsion is strongly reduced and reaches a flat minimum at $\phi \sim 18^\circ$. From the calculation, an orientation of benzene with two hydrogens pointing along the [1$\bar{1}$0] azimuth, i.e. rotated by 30°, would also be possible. Such an arrangement, however, would imply

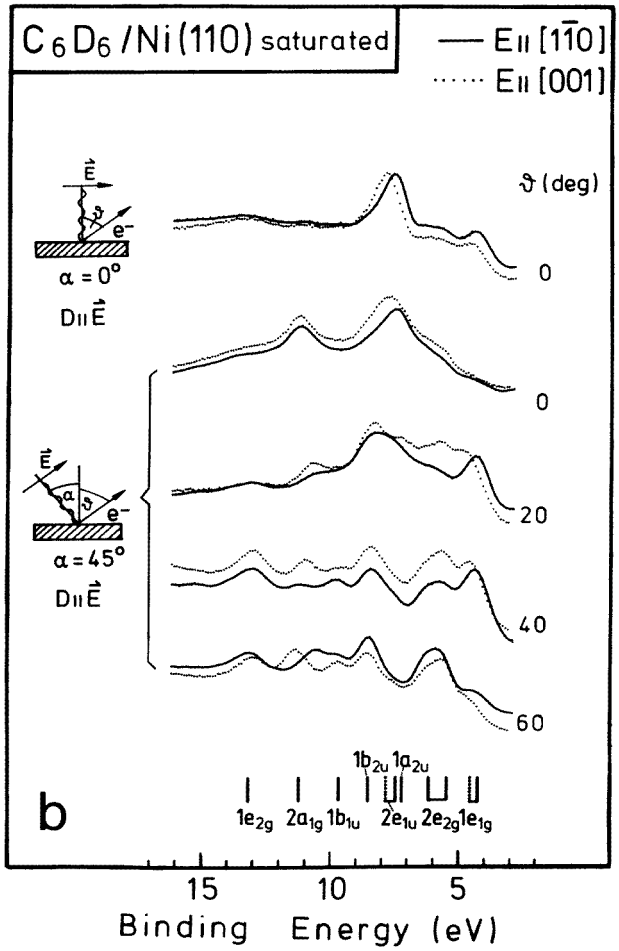

Figure 8. (Continued)

an alignment of the molecular mirror planes with the substrate high-symmetry directions (figure 10, III) which is ruled out by the non-zero intensity of both the $1b_{1u}$ orbital and the $1b_{2u}$ orbital for $\alpha = 45^\circ$ for both azimuths in figure 8(b). In conclusion, we thus propose the adsorption geometry shown in figure 9(b) and in figure 10, II, which results from the competition between the bonding of the molecule to the substrate (that favours the geometry of the isolated molecule) and repulsive lateral interactions [63]. The lateral interactions are also reflected in the dispersion of the $2a_{1g}$ benzene level due to the formation of a two-dimensional adsorbate band structure (see section 6.1).

4.3. Benzene/Ni(111)

The situation for benzene on Ni(111) [65] is quite similar to that on Ni(110). I will refrain from a detailed discussion of the ARUPS spectra but only present the key results of their analysis [39, 65]: independently of coverage, benzene adsorbs in a parallel adsorption geometry. In the dilute layer ($\theta = 0.3$–$0.8\,\theta_{SAT}$), the molecules are azimuthally oriented

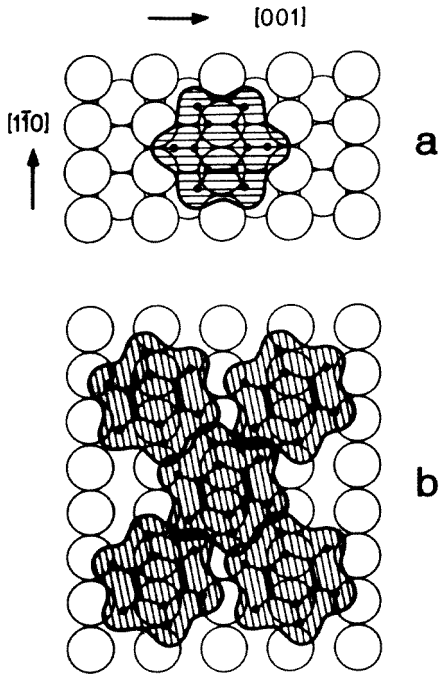

Figure 9. A schematic drawing of the proposed orientation of (a) a single benzene molecule in the dilute layer on Ni(110) and (b) the saturated c(4 × 2) benzene layer on Ni(110). Note that the adsorption site has been chosen arbitrarily [63].

with two C–H bonds pointing along the substrate [$\bar{2}$11] directions (figure 11(a), I). If the coverage is increased to its saturation value of $\theta_{SAT} = 0.143$ ML, where a well ordered $(\sqrt{7} \times \sqrt{7})$R19.1° LEED pattern is observed, we find a reorientation of the molecules as compared to the geometry in the non-saturated layer (figure 11(a), II) which is again attributed to lateral interactions: from simple steric arguments one concludes that the overlap of neighbouring molecules is reduced by the azimuthal rotation; in other words, an optimized packing of the molecules on the surface can only be obtained by reorienting the molecules to minimize lateral repulsion in the adsorbate layer [65]. This azimuthal reorientation has very recently been verified by a photoelectron diffraction study by Schaff *et al* [73], who find a bridge adsorption site at low coverage and a hcp hollow site at saturation; the hcp hollow site for the saturated layer is independently confirmed by Held *et al* using LEED [74]. The azimuthal reorientation is related to a order/disorder phase transition from the well ordered $(\sqrt{7} \times \sqrt{7})$R19.1° layer at saturation coverage to a disordered layer at lower coverages. This transition is also accompanied by a very sharp molecular benzene desorption peak at 294 K that is connected to the disappearance of the $(\sqrt{7} \times \sqrt{7})$R19.1° LEED pattern [40].

4.4. Benzene coadsorption with electronegative coadsorbates

The coadsorption of benzene with electronegative coadsorbates leads to the formation of well ordered mixed layers (see, e.g., references [39, 40, 57–68]) that in many cases are very stable and thus well suited as model systems for LEED, STM, HREELS and ARUPS studies. We have investigated the coadsorption of benzene with CO, NO and O on Ni(111) [39, 40,

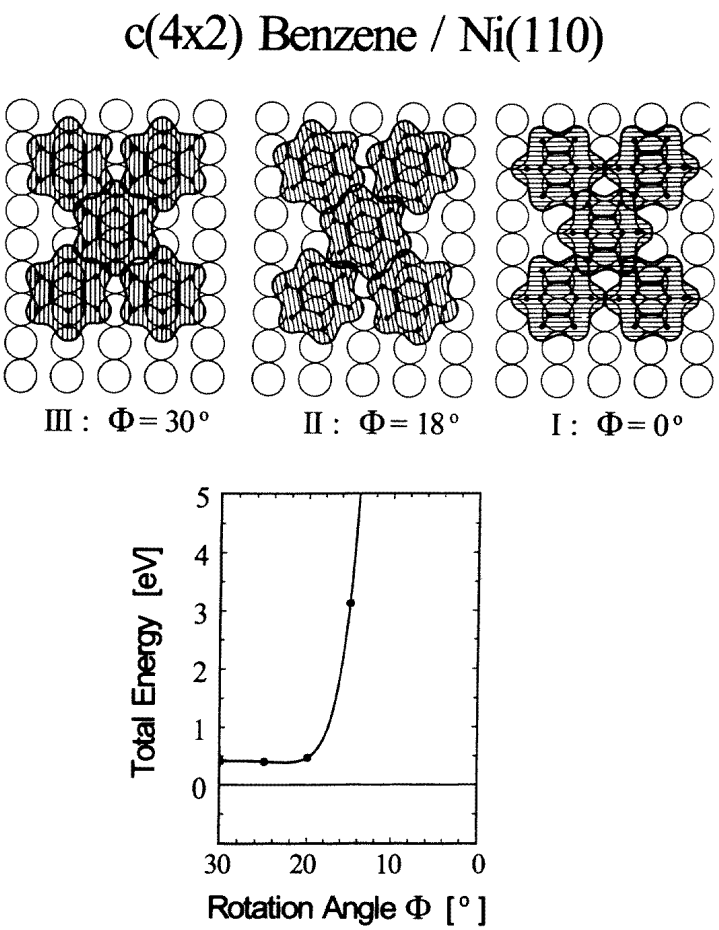

Figure 10. Top: the real-space arrangement for the saturated benzene layer on Ni(110) based on a c(4×2) structure [63]. I: two hydrogens along [001]—as in the dilute layer; II: azimuthally rotated by $\sim 18^\circ$ as compared to I; III: two hydrogens along $[1\bar{1}0]$ rotated by 30° as compared to I. Bottom: the force-field calculation of the repulsive energy per molecule for an unsupported benzene layer with the lateral arrangement of the c(4×2) layer on Ni(110) [77].

65], Ni(110) [63] and Ru(001) [66, 67]. Overall, the electronic structure of benzene in the coadsorbed layers is very similar to that of a pure benzene layer on the same surface. The only major differences in the spectra, apart from additional intensity due to the coadsorbate valence levels, are uniform shifts of the benzene levels towards lower binding energies which are attributed to electrostatic initial-state shifts. Only for benzene + NO on Ru(001) have we observed differential shifts of some levels, indicative of some additional changes in the chemical interaction [66, 67].

The detailed studies of the azimuthal orientation of benzene in coadsorbed layers show that azimuthal reorientation due to lateral interactions is not only restricted to pure benzene layers, but is also observed for benzene in coadsorbate layers: in loosely packed, mixed layers the molecules are oriented as in the dilute pure layers, whereas for very densely packed structures azimuthal reorientation due to steric reasons occurs, similar to the situation for pure benzene layers [65]. This is illustrated in figure 11(b), where the lateral arrangement

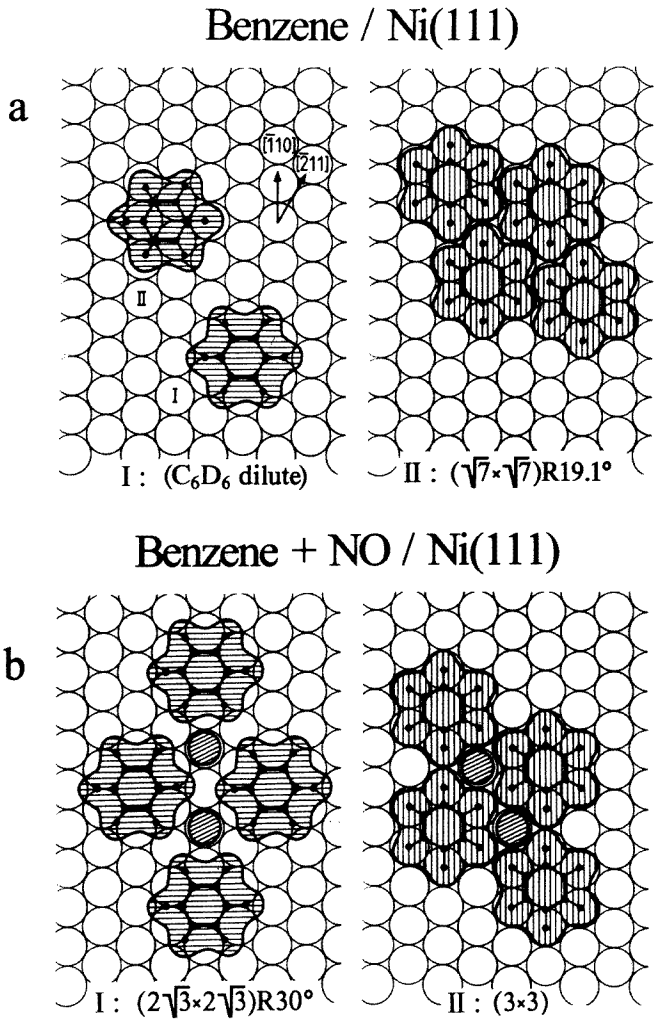

Figure 11. A schematic drawing of the adsorption geometry of pure and coadsorbed benzene layers on Ni(111) [65]. (a) I, a dilute layer with two possible adsorption sites; (b) I, a saturated $(\sqrt{7}\times\sqrt{7})$R19.1° layer; (a) II, $(2\sqrt{3}\times 2\sqrt{3})$R30° benzene + 2NO; (b) II, (3×3) benzene+2NO. Note that the adsorption site has been chosen arbitrarily.

of benzene + NO on Ni(111) is depicted for the well ordered $(2\sqrt{3}\times 2\sqrt{3})$R30° and (3×3) layers.

4.5. Benzene adsorption on a strongly corrugated surface

While for benzene adsorption on most low-index transition metal surfaces a flat adsorption geometry is reported that is attributed to the interaction of the benzene out-of-plane π-orbitals with the substrate atoms, the situation is not clear for strongly corrugated surfaces, such as the reconstructed Pt(110)1×2 surface. The surface reconstruction is of the missing-row type, i.e. every second closed-packed row of the topmost surface layer is missing. Previous studies of benzene adsorption on this surface at room temperature have shown

no ordered adsorbate layers, and a flat adsorption geometry was derived from HREELS measurements [55, 56]. We have investigated the adsorption of benzene on the reconstructed Pt(110)1×2 surface at low temperatures by ARUPS, accompanied by NEXAFS, XPS, LEED and TPD measurements [69].

At 100 K benzene is molecularly adsorbed on the Pt(110)1 × 2 surface. The saturated layer is disordered and corresponds to a coverage of ∼0.28 ML (1 ML = 1 adsorbate molecule/substrate atom of the non-reconstructed surface). Annealing to 280 K leads to partial benzene desorption and to the formation of a well ordered (4 × 2) layer (relative to the unreconstructed surface) with a coverage is 0.25 ML. From the missing $((2n+1)/4, 0)$ adsorbate LEED spots along $[1\bar{1}0]$ we deduce a glide plane in the adsorbate structure and the existence of two molecules per unit cell.

In figure 12 selected ARUPS spectra of the (4×2) layer are shown for normal incidence ($\alpha = 0^\circ$). Overall, the spectra exhibit the features typical for molecularly adsorbed benzene. At normal exit ($\vartheta = 0^\circ$) the $2a_{1g}$ level ($E_B = 11.1$ eV) shows no emission for $\boldsymbol{E}\|[1\bar{1}0]$ (along the substrate rows), but significant intensity for $\boldsymbol{E}\|[001]$ (perpendicular to the rows). From the non-vanishing $2a_{1g}$ intensity for $\boldsymbol{E}\|[001]$ we conclude that the molecular plane is tilted into the troughs. Further information on the azimuthal orientation is derived from the behaviour of the b-type orbitals in figure 12: from the vanishing intensity of the $1b_{1u}$ level ($E_B = 10.0$ eV) for $\boldsymbol{E}\|[001]$ in the allowed geometry (D$\|\boldsymbol{E}$) and its significant emission for both azimuths in the forbidden geometry (D $\perp \boldsymbol{E}$) we conclude that the σ_d-mirror plane of the molecule (the mirror plane intersecting the C–C bond) is aligned perpendicular to the rows, i.e. that two C–H bonds point along the $[1\bar{1}0]$ directions. The symmetry of the adsorption complex is C_s. The behaviour of all other levels is consistent with this symmetry.

This tilted adsorption geometry is further supported by NEXAFS measurements [69]. From the adsorbate coverage, the glide plane in the LEED pattern and the conclusions derived from ARUPS and NEXAFS we deduce an adsorption geometry as shown in figure 13, with the molecules tilted into the troughs of the reconstructed Pt(110)1 × 2 surface. For steric reasons and also from the existence of the glide plane we propose that the molecules are alternately adsorbed on opposite sides of the troughs. The tilt angle of $27^\circ \pm 10^\circ$ estimated from NEXAFS [69] roughly corresponds to the inclination angle (∼35°) of the (111) microfacets of the reconstructed (110) surface. This indicates a 'planar' adsorption geometry of benzene with respect to these microfacets, i.e. a 'local' orientation of the molecules similar to that on low-index transition metal surfaces. The driving force for this arrangement is the optimized overlap of the benzene π-orbitals with the electronic metal states in this geometry [69].

5. Electronic structure and bonding

Detailed information on the nature of the bond between the adsorbate and substrate can be derived from the energetic position of the molecular valence levels and in particular from differential shifts in the spectra due to the interaction with the substrate. In the examples discussed in the previous section we have always observed a bonding shift of the out-of-plane orbitals of the non-saturated hydrocarbon molecules that is attributed to the interaction of the respective molecular levels with the electronic states of the substrate. A more detailed understanding of the bonding interaction that goes beyond the qualitative arguments given above, can be obtained from quantum chemical model calculations. These calculations refer to the interaction between single molecules and the substrate and should therefore be correlated with the measurements for a dilute layer, i.e. for situations where lateral interactions are not important. In the following we will discuss the results for ethylene

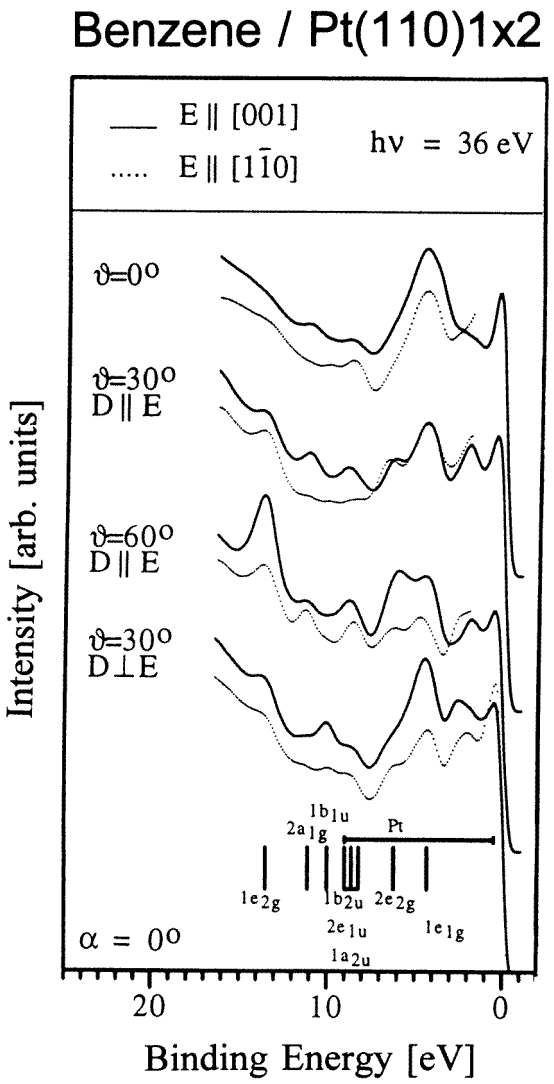

Figure 12. Angle-resolved UPS spectra of the (4×2) benzene layer on Pt(110)1×2, collected at a photon energy of 36 eV and an incidence angle α of 0°, for different polar angles ϑ. The plane of detection D is either parallel to the electric field vector $\boldsymbol{E}$ (D$\|\boldsymbol{E}$) or perpendicular to it (D $\perp \boldsymbol{E}$) [69].

and acetylene on Ni(110) with particular emphasis on the understanding of the electronic structure and the chemical bond to the substrate.

5.1. Ethylene/Ni(110)

The analysis of the ARUPS spectra of the dilute layer (figure 4 and figure 5(a)) reveals a bonding shift of the π-orbital $1b_{2u}$ of 1.1 eV, indicative of chemisorption on the substrate [31, 48]. In order to simulate the chemical bond of ethylene to Ni(110), LCGTO-LDF model cluster calculations have been performed for model clusters of various size simulating both

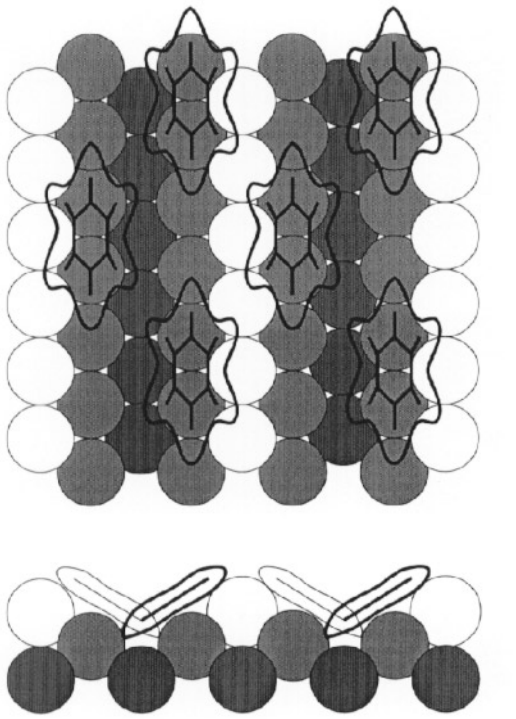

Figure 13. The proposed structure of benzene on the reconstructed Pt(110)1 × 2 surface as deduced from the ARUPS spectra in figure 12 and from NEXAFS and LEED [69].

di-σ- (bridge) and π- (on-top) adsorption geometries [31], with the C–C axis oriented along the substrate rows (figure 14(A)) as has been deduced from ARUPS spectra (see above). The key results from this calculation are summarized in table 3. Interestingly, the optimized geometries for the two bonding situations yield rather similar Ni–C and C–C distances, namely 2.06 Å and 1.41 Å for the di-σ-geometry, and 2.01 Å and 1.42 Å for the π-geometry, respectively [31]. In both cases the CH_2 out-of-plane bending angle is calculated to be 23°. The apparent insensitivity of the calculated bonding geometry to the adsorption site is attributed to the dominant contributions of the delocalized Ni 4s and 4p electrons to the dative ethylene/Ni bond (figure 14(B), c, d). Metal–adsorbate backdonation, on the other hand, relies on Ni 3d contributions (figure 14(B), a, b) [31]. The calculated binding energies favour the π-coordination ($E_B = 1.80$ eV) versus the di-σ-coordination ($E_B = 1.26$ eV), in contrast to the conclusion derived from HREELS [50].

5.2. Acetylene/Ni(110)

The adsorption of acetylene on metal surfaces has been investigated in great detail for various transition metal surfaces (see [42, 47, 50, 51, 78–80] and references in [81]). The bonding interaction of acetylene with the substrate is classified into two categories characterized by two different sets of vibrational frequencies [47]. The difference between these two types is associated with the bond order of the intramolecular C–C bond. Due to the interaction with the substrate, the degree of hybridization of the C atoms is assumed to change from

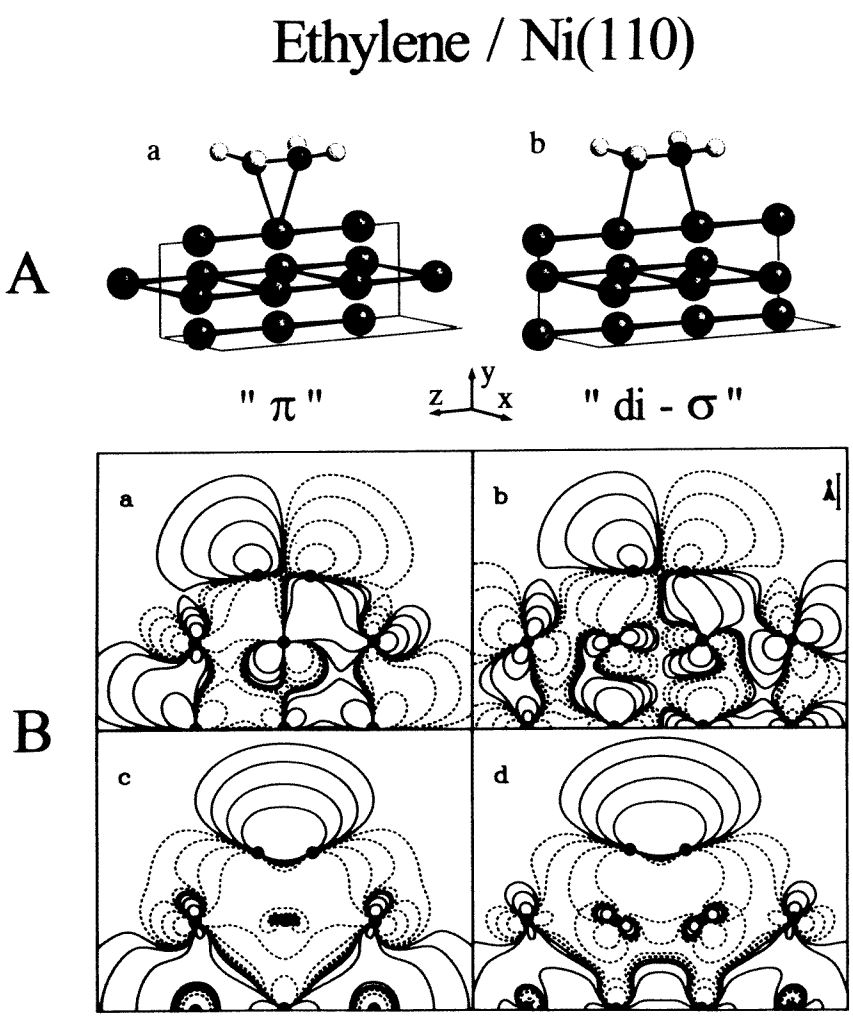

Figure 14. (A) Ni_{14} clusters modelling the chemisorption of ethylene on Ni(110): (a) π-geometry; (b) di-σ-geometry. The clusters used in the geometry optimization are supplemented to D_{2h} symmetry by a second adsorbate molecule. Reflection by the mirror plane at the 'bottom' of each cluster generates the large cluster models Ni_{25} and Ni_{24} that were used in the bonding analysis [31]. (B) A comparison of orbitals involved in the adsorption bond for the large cluster models Ni_{25} (π) and Ni_{24} (di-σ). π^*-backdonation in π- (a) and di-σ- (b) geometry; π-donation in π- (c) and di-σ- (d) geometry. The orbitals are shown in the yz-plane. The values of the contour lines follow a geometric progression with a factor $10^{1/2}$ starting at 10^{-3}; opposite signs are indicated by solid and dashed lines. The positions of the atoms are indicated by filled circles [31].

sp in the free molecule to sp^2 and beyond [47]. Furthermore, different adsorption sites and different structures of the adsorption complex, such as bent, bent and twisted, as well as tilted acetylene molecules, have been proposed for on various transition metal surfaces [47]. For Ni(110) Bandy *et al* deduce a di-$\sigma + \pi$-type interaction with the substrate with extensive rehybridization ($sp^{2.5}$) from HREELS [78]. Using the same method, Stroscio *et al* [50] propose a *trans*- or *cis*-bent acetylene species with different environments for the two C–H

Table 3. Comparison of the results of the LCGTO-LDF model cluster calculation for the $Ni_{14}(C_2H_4)$ clusters with di-σ- and π-geometry (figure 14) [31]. In addition, the experimental results for C_2H_4/Ni(110) [31] and for free ethylene are denoted.

	Metal–C (Å)	C–C (Å)	$\gamma(CH_2)$ (deg)
di-σ (Ni_{14})	2.06	1.41	23
π (Ni_{14})	2.01	1.42	23
Experiment (NEXAFS)	—	1.46 ± 0.05	—
Gas phase	—	1.34	0

groups adsorbed on a μ-bridging adsorption site, i.e. an orientation of the C–C axis along the [001] azimuth, in accord with the earlier model proposed by Demuth [79]. However, none of these studies contains direct information on the orientation and/or symmetry of the adsorption complex (as could be obtained, e.g., by additional off-specular HREELS or angle-resolved UPS) and thus, to a certain degree, these models had to be regarded as tentative. In the following we will review very recent experimental and theoretical results that have led to an significantly modified and improved understanding of this adsorption system [81].

Acetylene is molecularly adsorbed on Ni(110) at 100 K with a saturation coverage of $\sim$0.5 ML [81]. Starting at $\sim$50% of saturation, a c(2×2) LEED pattern is observed up to saturation coverage indicative of the formation of two-dimensional islands, significantly below saturation. In contrast to the case for ethylene and benzene it is therefore not possible to study the properties of the isolated molecule. Nevertheless, detailed information on the chemical bond to the surface as well as the orientation of the adsorbed molecules can be derived from the ARUPS data, in combination with NEXAFS, LEED and quantum chemical calculations [81]. The interpretation of the ARUPS spectra is however significantly more complicated than for ethylene and benzene. For an overview of the symmetry and the spatial extension, the molecular orbitals of acetylene are illustrated in figure 15, after Jorgensen and Salem [75].

A selected set of ARUPS spectra for the saturated c(2×2) acetylene layer on Ni(110) is depicted in figure 16 [81]. From the analysis of their polarization, polar angle and azimuthal dependence it is concluded that the molecules are oriented with the C–C axis parallel to the surface and preferentially aligned along the substrate troughs (the $[1\bar{1}0]$ azimuth); this geometry is schematically shown in figure 17. Here we will concentrate on the binding energies and assignment of the various levels, to obtain insight into the nature of the chemical bond. The various peaks show significant changes in binding energy with emission angle (i.e. dispersion), indicative of the formation of a 2D band structure.

The ARUPS spectra in figure 16 exhibit six distinct photoemission peaks [81]. For comparison, the UPS spectrum of condensed acetylene is shown at the bottom of figure 16 [82]; the spectrum has been shifted such that one obtains best alignment for the three peaks with the highest binding energies which are expected not to contribute strongly to the interaction with the substrate. These three peaks are identified as the $2\sigma_g$-, $2\sigma_u$- and $3\sigma_g$-orbitals of molecularly adsorbed acetylene. The corresponding binding energies at normal emission (the $\bar{\Gamma}'$ point, $|\boldsymbol{k}_\parallel| = 0$) are 16.8 eV, 11.2 eV and 9.0 eV, respectively. The assignment of the remaining three peaks cannot be simply derived from a comparison to the spectrum of gaseous or condensed acetylene since the spectrum of the free acetylene molecule contains only one more peak in that energy range, which is due to emission from

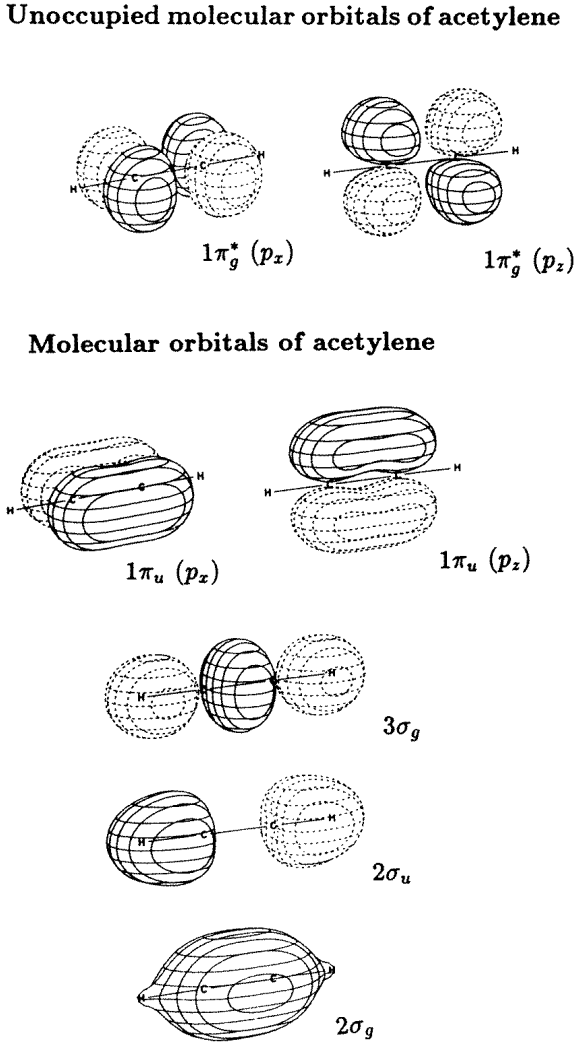

Figure 15. Molecular orbitals of acetylene after Jorgensen and Salem [75].

the twofold-degenerate $1\pi_u$-orbital (figure 15). We propose that this degeneracy is lifted by the adsorbate/substrate interaction which leads to a splitting of the $1\pi_u$-orbitals; due to additional adsorbate/adsorbate interaction the splitting depends on the parallel momentum, $\boldsymbol{k}_\parallel$, of the emitted electrons [81]. The two peaks in the binding energy range between 6.0 eV and 7.5 eV are assigned to emission from these p_x- and p_z-derived $1\pi_u$-bands (the y-direction is taken along the C–C bond of acetylene and the z-direction perpendicular to the surface). Because of the observed dispersion and mixing of the various levels we are not able to simply separate differential shifts of the individual orbitals. By comparison to the gas-phase spectrum, we obtain a differential shift of the centre of the $1\pi_u$-derived bands by 2.4 eV to higher binding energies. By taking into account this shift and the combined width of the band (1.4 eV) we deduce that both the x- and the z-component of the $1\pi_u$-level are shifted differentially with respect to the gas-phase value. From the differential

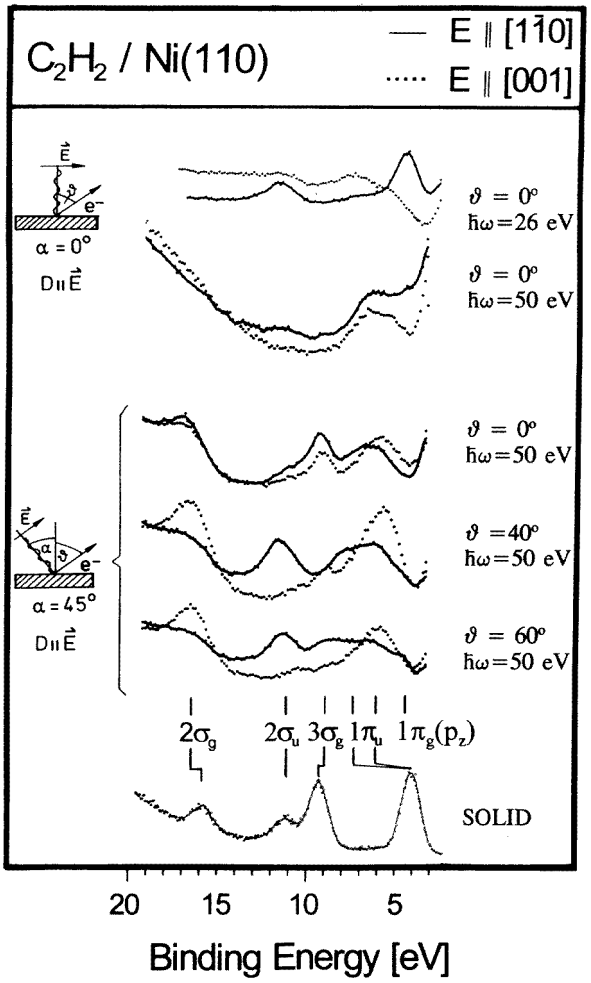

Figure 16. Selected ARUPS spectra of the saturated c(2×2) acetylene layer Ni(110) at different geometries, collected at photon energies of 26 and 50 eV [81]. Orbital positions and assignments are indicated as a bar diagram. D indicates the plane of detection, $\boldsymbol{E}$ the orientation of the electric field vector. At the bottom of the figure, a UPS spectrum of solid acetylene [82] is shown, aligned with respect to the adsorbate spectrum (see the text).

shift of both $1\pi_u$-derived orbitals we conclude that both are involved in the bonding to the substrate, indicating a highly coordinated adsorption site. Taking into account the derived orientation of the molecules we therefore propose that acetylene is adsorbed in the troughs of the Ni(110) substrate.

The additional peak at 4.5 eV that has no counterpart in the spectrum of the free molecule is attributed to the p_z component of the formerly unoccupied $1\pi_g^*(p_z)$ orbital (figure 15) that is shifted down below the substrate d manifold by the chemical interaction with the substrate. The assignment to a $1\pi_g^*(p_z)$-derived state is consistent with its polarization and polar-angle dependence [81] and is confirmed by theoretical cluster and slab model studies that have been performed for various possible adsorption sites: the cluster calculations include di-σ- and π-adsorption geometries with the C–C axis along [1$\bar{1}$0] and the molecule adsorbed

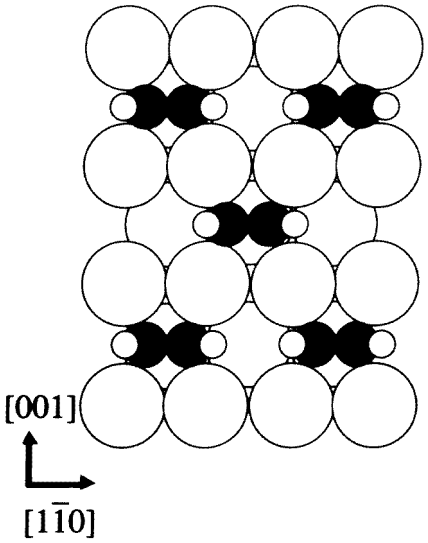

Figure 17. A schematic drawing of the adsorption geometry of acetylene on Ni(110) as derived from ARUPS, NEXAFS, LEED, and cluster and slab calculations [81].

on the rows, an adsorption site in the troughs of the Ni(110) surface with the C–C axis along [1$\bar{1}$0], and a μ-bonding site with the molecule adsorbed on the short bridge of the rows and the C–C axis perpendicular to the troughs, i.e. along [001]. These geometries are schematically illustrated in figure 18. The calculations have been performed at the LDF level and also using gradient corrections (GC) [81]. According to the binding energies, the trough geometry seems favoured by about 0.3 eV for the LDA calculations, while applying gradient corrections, the adsorbate is most strongly bonded (by about 0.3 eV) in the μ-geometry. However, since the energetic differences between the various structure models are rather small, no conclusive statement concerning the adsorption geometry can be deduced from the binding energies alone. Comparing the one-particle spectra of the various cluster models and the band structure of the corresponding slab models [81], the formerly unoccupied $1\pi_g^*(p_z)$ orbital below the substrate d band is only reproduced for the trough geometry. At the GC level of theory the optimized geometry parameters for the latter geometry are 2.02 and 2.19 Å for the distance between carbon atom and the first- and second-row nickel atoms, respectively, 1.42 Å for the C–C distance and 56° for the CH bending angle with respect to the substrate plane. The relatively long C–C bond length (that is in good agreement with the value determined from NEXAFS, 1.43 ± 0.05 Å [81], and the large bending angle indicate a strong degree of hybridization of the C atom of sp^2 or beyond.

6. Adsorbate band structures

The formation of adsorbate band structures in adsorbate layers was reported very early for CO on Ni(100) and Pd(100) by Horn *et al* [83–86]. Later on, systematic investigations, in selected cases accompanied by model calculations, followed for ordered CO layers on a variety of different substrates (for an overview, see references [11, 14]). For larger than diatomic molecules, such as hydrocarbons, the formation of adsorbate band structures

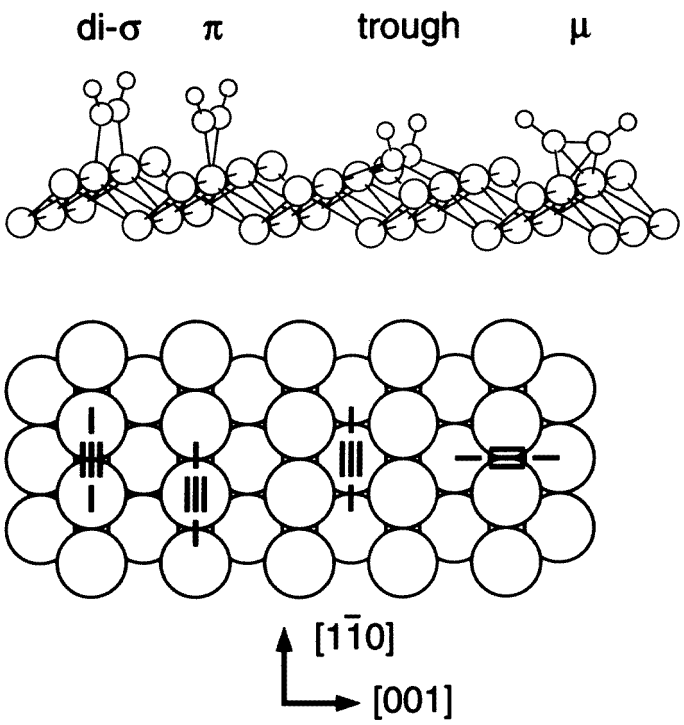

Figure 18. Cluster models for acetylene adsorbed on Ni(110) [81].

has however been neglected until recently. In this section, we will discuss the electronic structure of well ordered and densely packed hydrocarbon layers to demonstrate that for these systems the formation of a two-dimensional adsorbate band structure has to be taken into account, if one wants to describe the adsorption system correctly. I will concentrate on those adsorbates that we have already dealt with in this article, namely benzene and ethylene adsorbed on the Ni(110) surface. This is not only due to simplicity of presentation but also due to the fact that it is these systems that have been investigated in most detail [49,63]. Investigations on a fcc(110) surface with C_{2v} symmetry have the advantage that the data analysis is not hampered by the existence of symmetry-equivalent domains, in contrast to, e.g., the fcc(111), fcc(100) and hcp(001) surfaces; therefore the adsorbate bands can be measured up to $\boldsymbol{k}_{\parallel}$ in the second or sometimes even higher Brillouin zones.

*6.1. c(*4 × 2*) benzene/Ni(110)*

The saturated benzene layer on Ni(110) exhibits a c(4 × 2) LEED pattern (see section 4.2). The corresponding adsorbate surface Brillouin zone (SBZ) is shown in figure 19(a) [63]. From the dense packing of this layer one expects the formation of an adsorbate band structure. The detailed analysis of the ARUPS spectra at various emission angles and photon energies [63] indeed reveals a significant dispersion of the $2a_{1g}$ level with the emission angle. The corresponding two-dimensional adsorbate band structure has been determined from the spectra according to equation (5) and is plotted in figure 19(b) along the [1$\bar{1}$0] and [001] azimuths. The $|\boldsymbol{k}_{\parallel}|$-values of the symmetry points in the adsorbate SBZ are also marked in figure 19(b). The different symbols represent data collected at different photon energies.

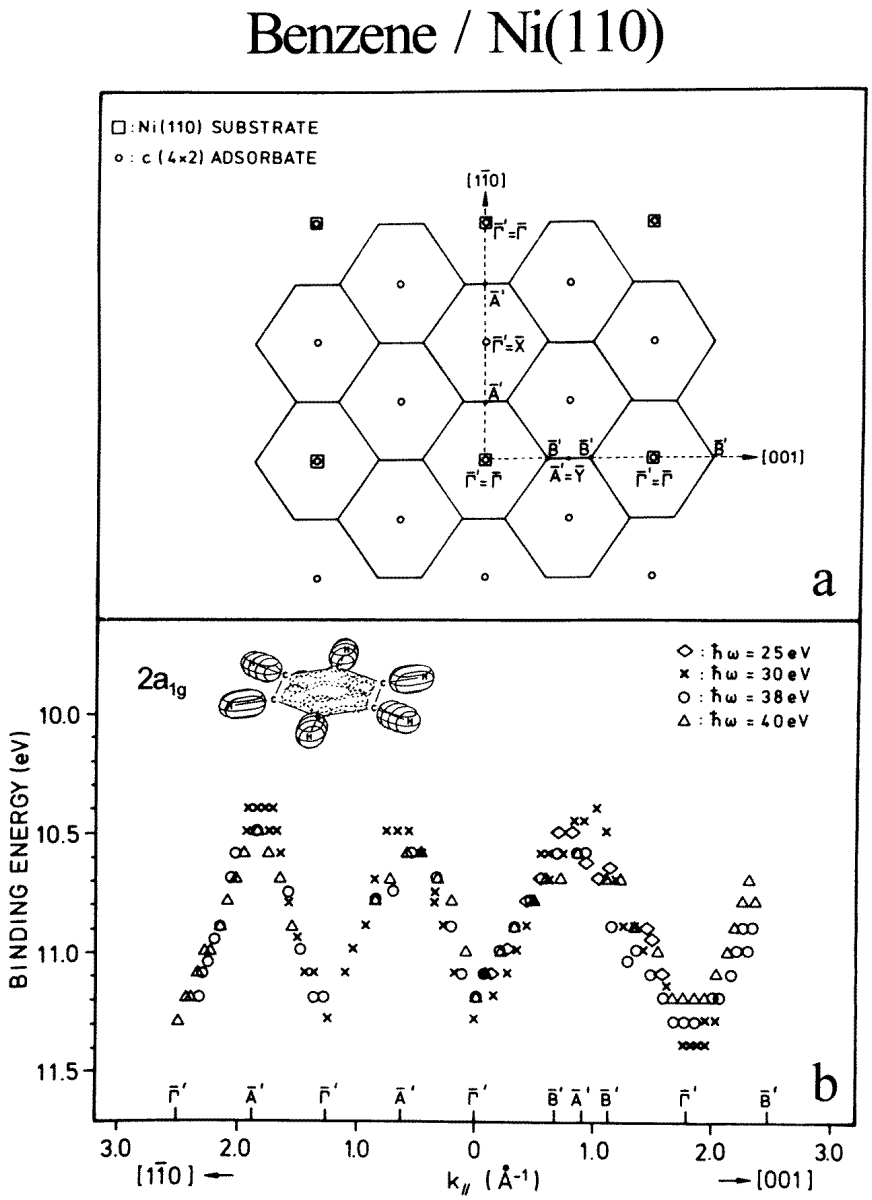

Figure 19. (a) The adsorbate surface Brillouin zone for a c(4 × 2) adsorbate structure; (b) the two-dimensional band structure of the saturated benzene layer on Ni(110) [63]; the inset in (b) shows the $2a_{1g}$ orbital of benzene [75].

The binding energy at the $\bar{\Gamma}'$ point is 11.3 eV; the magnitude of the dispersion is 0.8 eV for both azimuths. The periodicity of the experimentally determined 2D band structure very nicely reflects that of the c(4 × 2) adsorbate Brillouin zone for both azimuths: along [1$\bar{1}$0] the $2a_{1g}$ band closely follows the periodicity $\bar{\Gamma}'\bar{A}'\bar{\Gamma}'\bar{A}'\bar{\Gamma}'$ to the second-neighbour adsorbate SBZ; along [001] the $2a_{1g}$ band exhibits the periodicity $\bar{\Gamma}'\bar{B}'\bar{A}'\bar{B}'\bar{\Gamma}'\bar{B}'$. The binding energy of the $2a_{1g}$ level at the $\bar{A}'$ point can thus be either obtained by measuring along [1$\bar{1}$0] or

[001], with the two values being identical (10.5 ± 0.1 eV), as should be the case. All other levels show no significant dispersion [63].

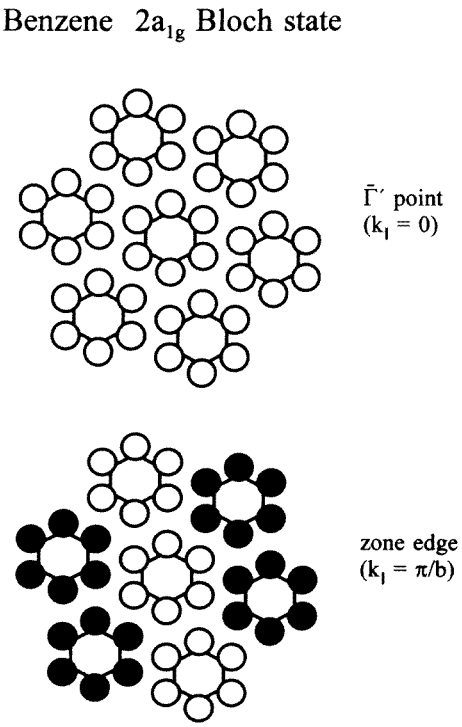

Figure 20. A schematic representation of the $2a_{1g}$ Bloch wave function of benzene molecules in a hexagonal arrangement for the $\bar{\Gamma}'$ point and the zone edge of the first Brillouin zone.

Investigations of densely packed, well ordered benzene layers on hexagonally close-packed transition metal surfaces have also shown the formation of two-dimensional band structures of the $2a_{1g}$ level: for $(\sqrt{7} \times \sqrt{7})$R19.1° benzene/Ni(111) [65], $(\sqrt{7} \times \sqrt{7})$R19.1° benzene/Os(001) [70] and $(\sqrt{19} \times \sqrt{19})$R23.4° benzene/Rh(111) [71] dispersions of ~0.4 eV have been observed; the result that the band width is smaller than the one observed for Ni(110) is attributed to larger nearest-neighbour distances in these layers. Overall, the behaviour on those surfaces is, however, similar to that on Ni(110): the $2a_{1g}$-derived band is strongly bonding at the $\bar{\Gamma}'$ point and antibonding at the zone edge (the A$\bar{\Gamma}'$ point in figure 19). A qualitative understanding of this behaviour can be obtained by analysing the wavefunctions of neighbouring molecules for the two symmetry points: in figure 20 the $2a_{1g}$ Bloch wave functions are schematically indicated for the $\bar{\Gamma}'$ point and the zone edge of a hexagonal benzene layer. This geometry represents the arrangement on Ni(111) and Os(001) and is a fairly good approximation for the quasihexagonal c(4 × 2) structure on Ni(110). At the $\bar{\Gamma}'$ point, all wave functions are in phase; for the totally symmetric $2a_{1g}$ orbital this leads to a strongly bonding situation. At the zone edge the wave functions of two neighbours are in phase, while those of the other four neighbours have opposite phase, which leads to an antibonding situation. As a consequence we expect a significant upward dispersion from the $\bar{\Gamma}'$ point to the zone edge, as is observed in the experiment (figure 19(b)).

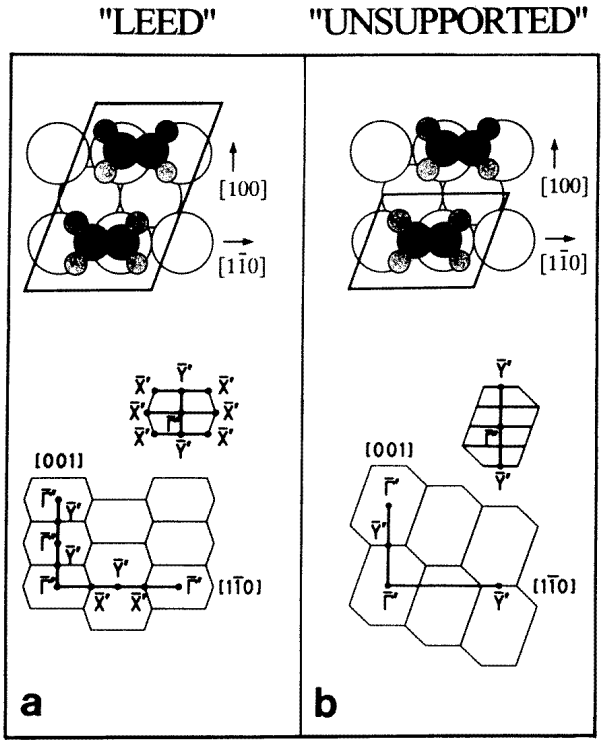

Figure 21. The extended Brillouin zone scheme for the ethylene c(2×4) structure on Ni(110) (a) as determined from the c(2×4) LEED pattern and (b) for the unsupported ethylene layer; this structure is obtained by simply neglecting the substrate in (a). The experimental $\boldsymbol{k}_{\parallel}$-paths along the [1$\bar{1}$0] and [001] azimuths of the Ni substrate are indicated as solid lines. The labels denote the high-symmetry points of the two structures. The real-space unit cells of the corresponding lattices are given at the top of the figure [49].

6.2. c(2 × 4) ethylene/Ni(110)

A very interesting example is the band structure of the saturated c(2×4) ethylene layer on Ni(110) [49]; the real-space structure of this compressed layer has been discussed in section 4.1 and is shown in figure 6(b). Translationally equivalent adsorption sites are occupied only every second row, entailing a non-primitive oblique unit cell of the c(2×4) structure. By neglecting the underlying substrate, one obtains however an adsorbate structure with a smaller unit cell containing only one molecule. The extended adsorbate Brillouin zone as deduced from the c(2×4) LEED pattern is illustrated in figure 21(a), and the larger adsorbate Brillouin zone for the isolated layer is shown in figure 21(b). The various symmetry points of both structures are also indicated.

The angle-resolved UPS spectra of the saturated c(2×4) ethylene layer (figure 5(b)) exhibit significant dispersion for several molecular levels [49]. The corresponding adsorbate band structure is evaluated along the [1$\bar{1}$0] and [001] directions of the substrate, and is depicted in figure 22. The highest-lying, $1b_{2u}$-derived band shows essentially no dispersion, which is attributed to its out-of-plane (π-) character. The $1b_{2g}$ and $2b_{1u}$ bands exhibit no dispersion along [001], but significant dispersion along [1$\bar{1}$0]. The $3a_g$ and $1b_{3u}$ bands show

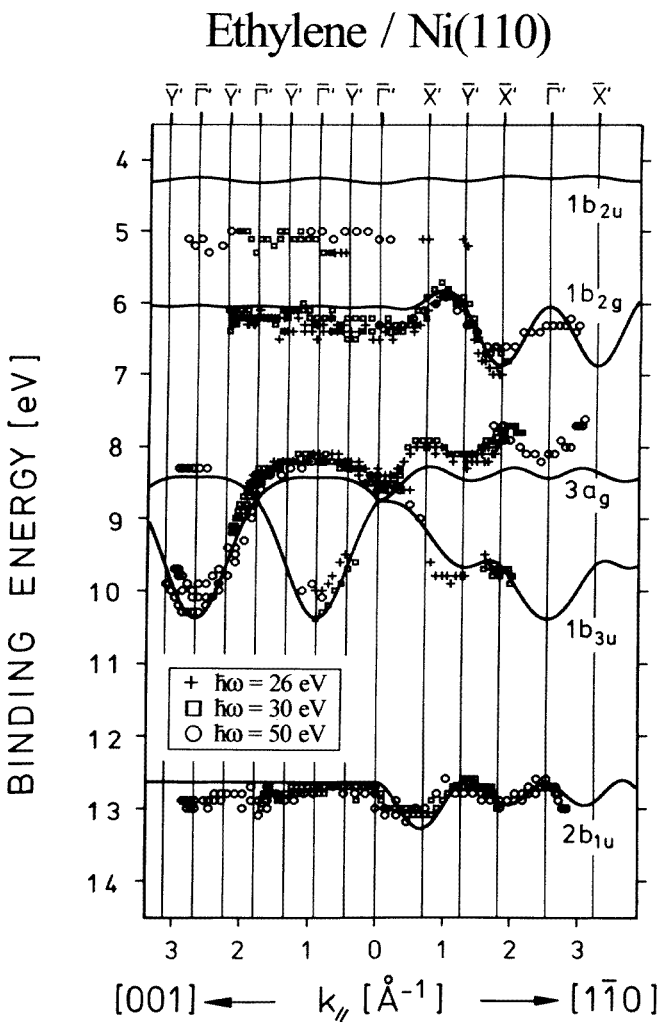

Figure 22. The 2D band structure of the saturated ethylene layer as determined from ARUPS spectra at various photon energies [49]: (+) 26 eV, (□) 30 eV, (○) 50 eV. The solid lines indicate the calculated band structure for an unsupported layer. The labels correspond to the high-symmetry points of the Brillouin zone as deduced from the c(2 × 4) LEED pattern (figure 21(a)).

dispersion for both azimuths. At the $\bar{\Gamma}'$ points ($|\boldsymbol{k}_{\parallel}| = 0$ Å^{-1} and $|\boldsymbol{k}_{\parallel}| = 1.8$ Å^{-1} along [001]) these two bands are energetically nearly degenerate, with the binding energy of the $1b_{3u}$ band being even somewhat smaller than that of the $3a_g$ band (8.4 versus 8.6 eV). The magnitude of the dispersion differs for the various bands; the highest value of 2 eV (!) is observed for the $1b_{3u}$ band.

The periodicity of the 2D adsorbate band structure of ethylene on Ni(110) does NOT reflect the symmetry of the adsorbate Brillouin zone deduced from the c(2 × 4) LEED pattern. Also, the detailed analysis of the ARUPS spectra reveals NO splitting (doubling) of any of the adsorbate bands that is expected from the existence of two non-equivalent molecules per unit cell. On the other hand, 2D band-structure calculations performed in

a tight-binding approximation at the extended Hückel level for the unsupported ethylene layer (only one adsorbate molecule per unit cell—figure 21(b)) are in excellent agreement with the measured bands [49]. This is evident from figure 22, where the calculated band structure is indicated as solid lines, aligned with respect to the $2b_{1u}$ band of the experimental data at the $\bar{\Gamma}'$ point. The complete measured energy dispersion is very well reproduced for all calculated bands. Small discrepancies are observed only for the $3a_g$ band, indicating the limits of the approximate band-structure method. The major difference between the experimental spectra and the calculation for the unsupported layer is the fact that—as is to be expected—the calculated π-derived band ($1b_{2u}$) lacks the substrate-induced bonding shift of about 0.8 eV to higher binding energies. The good agreement between the calculated band structure for the unsupported ethylene layer and the experimental results for the $c(2\times4)$ layer indicates that the 2D adsorbate band structure of the saturated ethylene layer on Ni(110) is dominated by the adsorbate/adsorbate interactions. The 'vertical' adsorbate/substrate interactions, which are responsible for the bonding of the molecule to the surface, are essentially decoupled from the lateral interactions and are reflected only in the differential shift of the out-of-plane π-orbital ($1b_{2u}$) that is mainly responsible for the bonding.

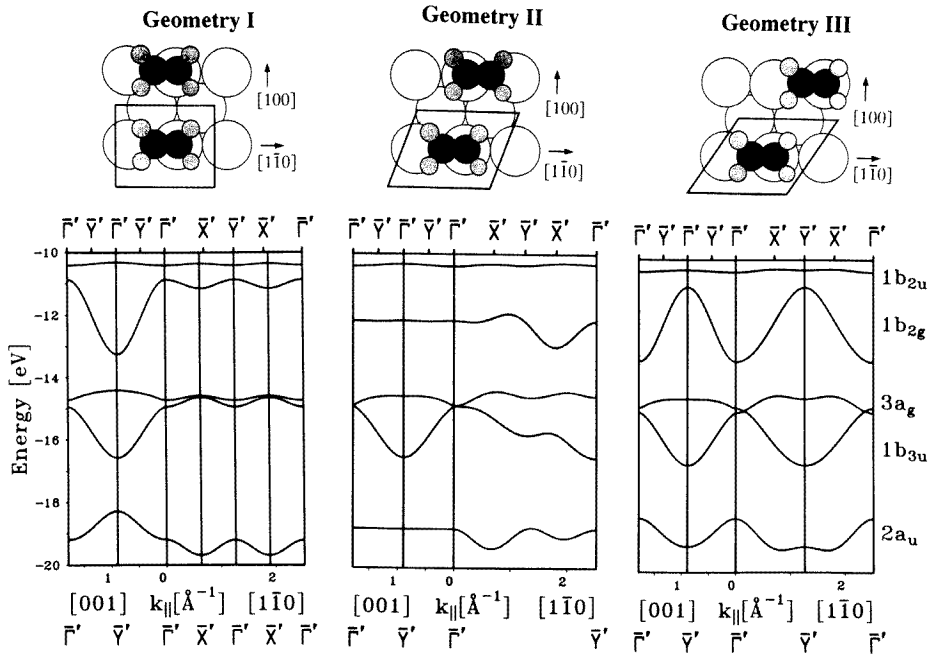

Figure 23. Band-structure calculations for the saturated (unsupported) ethylene layer with different lateral arrangements of the molecules [49]. In each case the relative position of neighbouring molecules is shown at the top of the figure with the unit cell of the corresponding lattice.

A very interesting aspect of the band-structure calculations is their sensitivity to the arrangement of the molecules on the surface. This sensitivity can be used to obtain additional information on the orientation of the molecules on the surface as well as the arrangement of neighbouring molecules [49, 81]. For ethylene on Ni(110) the band structure has been calculated for different positions of the molecules in neighbouring rows. The results of the calculation are shown in figure 23 for three different arrangements, denoted as geometries

I–III. Geometry II corresponds to geometry derived from ARUPS, NEXAFS, LEED and force-field calculations. The most dramatic changes with the geometry are observed for the $1b_{2g}$ and the $2a_u$ bands, in particular along the [001] azimuth [49]: the $1b_{2g}$ band exhibits a downward dispersion of ∼2.4 eV for geometry I, an upward dispersion of ∼2.4 eV for geometry III, but is completely flat for geometry II. The latter behaviour is observed in the experiment, which provides strong support for the structural model proposed in figure 6(b) [49].

7. Some special aspects

The adsorption of molecules on surfaces leads not only to changes in the initial state, but also influences the final state in the photoemission process. The investigation of these effects can provide additional insight into the nature of adsorbate/substrate interaction, and/or the photoemission process itself. In the following I will discuss some aspects concerning the photoionization cross section and vibronic coupling of molecules adsorbed on surfaces.

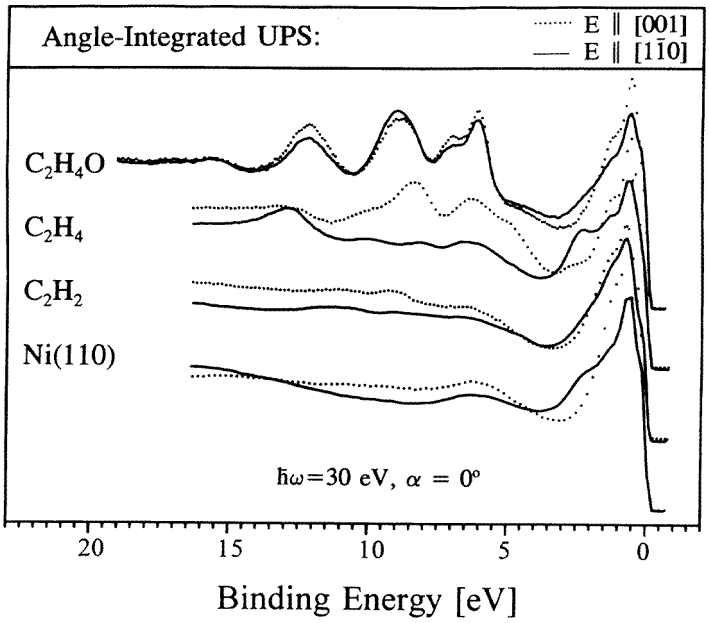

Figure 24. A comparison of angle-resolved UPS spectra of acetylene, ethylene and ethylene oxide, obtained under the same experimental conditions. The coverage in each case is 0.5 ML.

7.1. Photoionization cross sections

The differential cross section for the photoemission process strongly depends on the electronic structure of the subject investigated. Since the valence electronic structure of a molecule is modified upon adsorption on a surface, changes in the differential cross section are observed. These changes depend in a complicated way on the details of the adsorbate/substrate interaction. Furthermore, for a given experimental geometry the intensity of various peaks in the UPS spectra will strongly depend on the orientation of the adsorbate,

on the adsorption site, and on lateral interactions (see section 4). This is why the intensity of a valence peak can by no means be used as a measure for the adsorbate coverage. In addition, it is also not possible to derive conclusive information on adsorbate coverages by comparing the intensities of valence levels to those of a comparable adsorbate. This is evident from figure 24, where angle-integrated spectra of acetylene, ethylene and ethylene oxide are plotted [49, 81, 87, 88]; for all layers the adsorbate coverage was 0.5 ML, but the intensity of the valence levels is very different, roughly a factor of 5 smaller for acetylene than for ethylene oxide.

The photoionization cross sections of the various orbitals of free molecules can exhibit more or less pronounced maxima as functions of photon energy [89] that are commonly called shape resonances [90–94] and are attributed to intramolecular scattering resonances or to excitations to quasibound molecular orbitals. Both interpretations lead to completely equivalent conclusions [92, 93]. The interpretation of shape resonances as excitations from a particular occupied orbital to a quasibound orbital immediately implies a well defined symmetry of the final state. This allows one to draw conclusions about the symmetry of a particular final state in the experiment on the one hand, and on the other hand, for a given final state, additional information on the orientation of the adsorbate, due to symmetry selection rules. Arguments along these lines have been used for CO adsorbed on metal surfaces [95, 96].

In contrast to the case of CO on metal surfaces, only few investigations on adsorbed hydrocarbon molecules are available in the literature. In the following we will discuss the photoionization cross section of chemisorbed benzene layers on Ni(110) and Ni(111) [39, 63, 67]. In figure 25 ARUPS spectra for benzene on Ni(110) are depicted for various photon energies at normal incidence [63]. The $2e_{1u}$ level shows a pronounced maximum at a photon energy of 25 eV. This is even more evident in figure 25(B) where the $2e_{1u}$ intensity is plotted versus photon energy. At the resonance the emission of the $2e_{1u}$ peak is focused along the surface normal ($\vartheta = 0^\circ$), but at a polar angle of $\vartheta = 20^\circ$ it has strongly decreased (the corresponding spectra are included in figure 25(A) for $\bar{h}\omega = 25$ eV). A very similar result has been obtained for benzene on Ni(111) [39, 67].

On the basis of the focusing of the electron emission along the surface normal, the maximum in the $2e_{1u}$ photoionization cross section is attributed to a shape resonance in the continuum with a_1 symmetry. This assignment is supported by LCGTO-LDF calculations for free benzene that assign the resonance of the $2e_{1u}$ level to predominant excitations into a_{1g} and e_{2g} final states [97]. With respect to adsorption geometry, the very narrow width of the emission cone can be considered as strong evidence for the parallel orientation of the benzene molecule on Ni(110) and Ni(111). For a tilting of the molecules by more than $\pm 5^\circ$ this sharp peak should be significantly broader. The energetic position of the $2e_{1u}$ resonance for chemisorbed benzene at $\bar{h}\omega = 25$ eV ($E_{Kin} = 13$ eV) contrasts with the value of $\bar{h}\omega = 18$ eV for the isolated molecule [98]. Similar differences have however also been observed for CO, and have been attributed to differences in the hole screening mechanism [99].

Finally, I want to address an interesting point, where one can take advantage of the different energy dependencies of the cross sections of different valence levels to study the electronic structure in coadsorbate layers. As an example, ARUPS spectra of a coadsorbed ordered $(\sqrt{13} \times \sqrt{13})$R13.1° CO + benzene layer on Ru(001) are given in figure 26 along with spectra of pure CO and benzene layers [66, 67]. The 18 eV spectrum clearly emphasizes the benzene features while at 50 eV the CO-derived peaks dominate. The cross section variations allow, for example, the isolated observation of benzene band C at $\bar{h}\omega = 18$ eV and the CO 5σ-level at 50 eV which could otherwise not be resolved from each other.

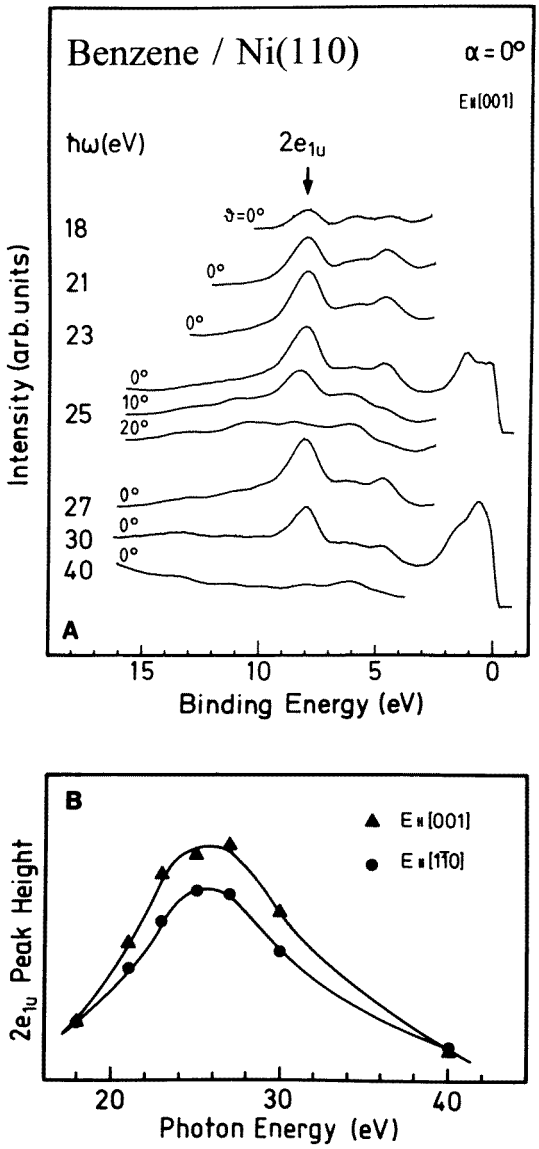

Figure 25. (A) A series of normal-emission spectra ($\vartheta = 0^\circ$) for the c(4 × 2) benzene layer ($\theta_{C_6D_6} = 0.25$ ML) on Ni(110) for various photon energies, at normal incidence [63]; for $\hbar\omega = 25$ eV the spectra for emission angles of $\vartheta = 10^\circ$ and 20° are also included. (B) The peak height of the $2e_{1u}$ level as obtained from angle-resolved UPS spectra.

7.2. Vibronic coupling

The UPS spectra of complex molecules can in some cases not be understood in terms of the simple Franck–Condon picture (reference [100]). For energetically close-lying orbitals vibronic coupling is observed with the coupling strength depending on the details of the potential-energy surface (reference [101]). In most cases no conclusions on the vibronic coupling can be derived for adsorbed molecules because the vibrational fine structure is

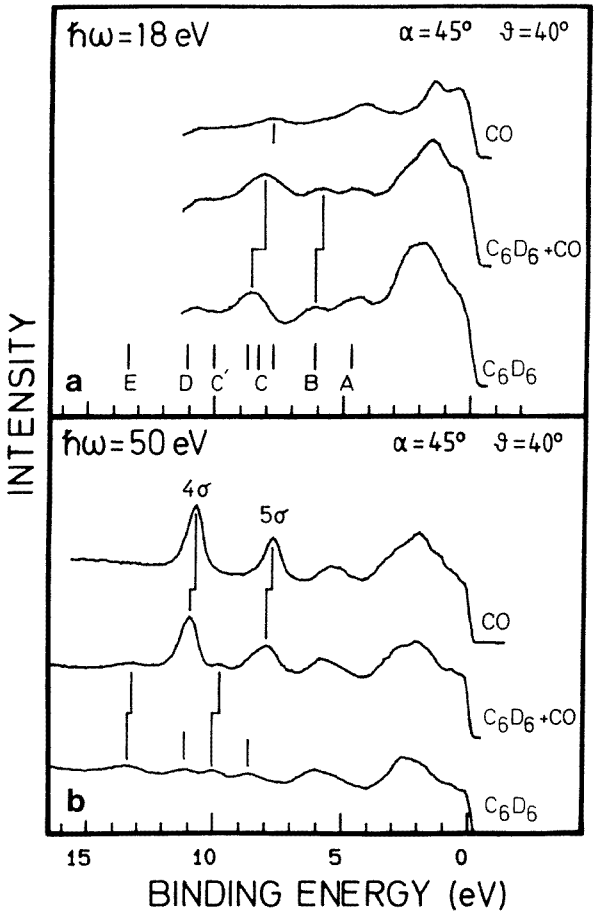

Figure 26. ARUPS spectra of benzene, CO, and coadsorbed CO + benzene at photon energies of (a) 18 eV and (b) 50 eV [66, 67]. The angle of incidence $\alpha = 45^\circ$; the emission angle $\vartheta = 40^\circ$.

broadened due to the interaction with the substrate (see section 2.1); however, in special situations the investigation of adsorbed molecules can, despite of the inherently lower resolution, provide novel information on the spectroscopy and dynamics of molecular cations. One of these examples is benzene adsorbed on metal surfaces (reference [102]).

In the majority of ARUPS investigations of benzene chemisorbed on transition metal surfaces, the $2e_{2g}$ level ($E_B = 6.3$ eV) exhibits a more or less well resolved double-peak structure (reference [103]) which is clearly visible in figure 1, figure 8 and even more evident in figure 27, where a selected ARUPS spectrum of benzene chemisorbed on Ni(111) is depicted on an enlarged binding energy scale [39, 102]. After the initial report by Lloyd *et al* [53] for benzene on Pd(100), Neumann *et al* [54] have attributed this double-peak structure to a Jahn–Teller (JT) effect, i.e. to a lifted degeneracy of the $2e_{2g}$ state of the ionized molecule (reference [104]).

This interpretation has recently been verified by Eiding *et al* (reference [102]): for the free molecule, the $2e_{2g}$ level is subject to a strong (pseudo-Jahn–Teller) vibronic interaction with the close-lying $1a_{2u}$ level, which strongly affects the vibronic structure of both levels

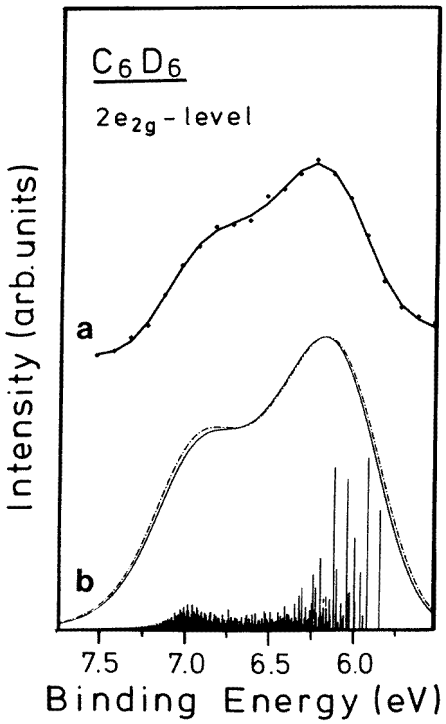

Figure 27. (a) A selected angle-resolved UPS spectrum of a saturated chemisorbed ($\sqrt{7} \times \sqrt{7}$)R19.1° C_6D_6 layer on Ni(111) on an enlarged energy scale (with respect to E_F). The angle of incidence $\alpha = 45°$; the emission angle $\vartheta = 60°$. (b) The calculated vibronic fine structure of the isolated $2e_{2g}$ hole state of free C_6D_6 obtained by including three JT-active vibrational modes (ν_6, ν_8, ν_9) as well as the totally symmetric modes ν_1, ν_2. The full curve shows the low-resolution band shape obtained by convolution with a Gaussian of 0.2 eV FWHM. Chain curve: the band shape obtained with the inclusion of all four JT-active vibrational modes, making use of the effective-mode approximation (reference [102]). Note that spectrum (b) is shifted on the binding energy scale to align with the experimental spectrum.

(reference [105]). For chemisorbed benzene the $1a_{2u}$ (π-) orbital is differentially shifted to higher binding energies (figure 1) and the $2e_{2g}$ orbital is observed as an isolated peak (figure 27(a)). One therefore can expect that the $2e_{2g}$–$1a_{2u}$ vibronic interaction can be neglected for chemisorbed benzene and treat the $2e_{2g}$ hole state as an isolated electronic state of the benzene cation. In order to investigate this behaviour in detail, *ab initio* quantum mechanical calculations of the vibronic spectrum of the isolated $2e_{2g}$ level of gas-phase benzene have been performed (reference [102]) to study the multi-mode dynamical Jahn–Teller effect in this specific molecular level. The resulting vibronic spectrum is shown as a line spectrum in figure 27(b). Simulating the various broadening mechanisms operative in benzene chemisorbed on metal surfaces by convolution with a Gaussian of 0.2 eV FWHM, one obtains the full curve in figure 27(b). The comparison shows very good agreement between the calculated low-resolution band shape and the experimentally observed band shape of the $2e_{2g}$ level for C_6D_6 on Ni(111). The calculated peak-to-shoulder separation at 0.6 eV is in full accord with the experimental observations. Similar calculations for C_6H_6 show differences in the line spectrum but virtually identical low-resolution band shape (reference [106]). In a semiclassical picture, this double-peak structure can be qualitatively

understood as arising from the two components of the adiabatic potential-energy surface split by the Jahn–Teller interactions (references [107, 108]).

8. Synopsis and outlook

Angle-resolved UV photoelectron spectroscopy is a very powerful tool for studying the properties of adsorbed hydrocarbons. In combination with theoretical calculations detailed information can be derived on the electronic structure and bonding to the substrate, on the orientation and symmetry of the adsorbate and the influence of lateral interactions, the formation of two-dimensional adsorbate band structures and on some special aspects concerning the photoemission process such as the photoionization cross section and vibronic coupling. These aspects have been discussed using several examples of simple hydrocarbon molecules, namely benzene, ethylene and acetylene adsorbed on Ni(110), Ni(111), Ru(001) and the reconstructed Pt(110)1×2 surfaces.

Finally, I shall briefly comment on the potential of angle-resolved UV photoelectron spectroscopy in the future. In my opinion, there are several aspects that will be important.

(1) The extended combination of experimental results with detailed quantum chemical calculations that strongly benefit from the increasing power of computers will provide a much deeper understanding of the electronic structure of adsorbed molecules and their bonding to the substrate.

(2) The adsorption of molecules on 'new materials' such as ultrathin metal films opens up a wide field, where a detailed knowledge of the electronic adsorbate structure is required which can be obtained by ARUPS. For these materials, the very well known properties of adsorbates on the solids can be used also as a tool to monitor the electronic structure of the substrate.

(3) Another very important application will be the possibility of measuring 'time-dependent' ARUPS spectra. Using the high-intensity photon beams that already are or will be available at third-generation synchrotron radiation sources, one should be able to collect ARUPS spectra on time-scales below one second. This will allow real-time *in situ* investigations of adsorption and desorption processes and of chemical reactions on surfaces.

Acknowledgments

I appreciate the cooperation with Dr W Huber, Dr M Weinelt and Dr P Zebisch who have done most of the experimental work presented here, and thank Professor Dr D Menzel for his continuing support during this work which has mostly been performed at the Technische Universität München, and for many stimulating discussions. I also want to acknowledge Professor Dr N Rösch, Dr B Reichert, Dr U Birkenheuer, M Pabst, P Ulbricht and Dr T Fox for fruitful collaboration, and M Glanz and K Eberle for technical support. I am grateful to the BESSY staff for their support. This work was supported by the BMFT through grants 05 466 CAB, 05 5WO CAI, 05 625 WWB and by the Deutsche Forschungsgemeinschaft through SFB 338.

References

[1] Cardona M and Ley L (ed) 1978 *Photoemission in Solids I* (New York: Springer); 1979 *Photoemission in Solids II* (New York: Springer)

[2] Feuerbacher B, Fitton B and Willis R F (ed) 1978 *Photoemission and the Electronic Properties of Surfaces* (New York: Wiley)

[3] Fiermans L, Vennik J and Dekeyser W (ed) 1978 *Electron and Ion Spectroscopy of Solids* (New York: Plenum)
[4] Smith N V and Himpsel F J 1983 *Handbook on Synchrotron Radiation* vol 1B, ed E-E Koch (Amsterdam: North-Holland)
[5] Ertl G and Küppers H 1985 *Low Energy Electrons and Surface Chemistry* (Weinheim: VCH)
[6] Woodruff D P and Delchar T A 1986 *Modern Techniques in Surface Science* (Cambridge: Cambridge University Press)
[7] Richardson N V and Bradshaw A M 1981 *Electron Spectroscopy—Theory, Techniques and Applications* vol 4, ed C R Brundle and A D Baker (New York: Academic)
[8] Plummer E W and Eberhardt W 1982 *Adv. Chem. Phys.* **49** 533
[9] Siegbahn H and Karlsson L 1982 *Handbuch der Physik XXXI* ed W Mehlhorn (Berlin: Springer)
[10] Scheffler M and Bradshaw A M 1983 *The Chemical Physics of Solid Surfaces and Heterogeneous Catalysis* vol 2, ed D A King and D P Woodruff (Amsterdam: Elsevier)
[11] Freund H-J and Neumann M 1988 *Appl. Phys.* A **47** 3
[12] Eberhardt W 1992 *Techniques (Synchrotron Radiation Research: Advances in Surface and Interface Science 1)* ed R Z Bachrach (New York: Plenum)
[13] Netzer F P 1990 *Vacuum* **41** 49
[14] Freund H-J and Kuhlenbeck H 1995 *Applications of Synchrotron Radiation (Springer Series in Surface Sciences 25)* ed W Eberhardt (Berlin: Springer)
[15] Steinrück H-P 1994 *Vacuum* **45** 715
[16] Steinrück H-P 1994 *Appl. Phys.* A **59** 517
[17] Netzer F P and Ramsey M G 1992 *Crit. Rev. Solid State Mater. Sci.* **17** 397
[18] Gadzuk J W 1974 *Surf. Sci.* **43** 44
[19] Gadzuk J W 1978 *Photoemission and the Electronic Properties of Surfaces* ed B Feuerbacher, B Fitton and R F Willis (New York: Wiley) ch 5
[20] Menzel D 1978 *Photoemission and the Electronic Properties of Surfaces* ed B Feuerbacher, B Fitton and R F Willis (New York: Wiley) ch 13
[21] Gadzuk J W 1976 *Phys. Rev.* B **14** 5458; 1979 *Phys. Rev.* B **20** 515
[22] Gadzuk J W, Holloway S, Mariani C and Horn K 1982 *Phys. Rev. Lett.* **48** 1288
[23] Norton P R, Tapping R L, Broida H P, Gadzuk J W and Waclawski B J 1978 *Chem. Phys. Lett.* **53** 465
[24] Fuggle J C and Menzel D 1979 *Surf. Sci.* **79** 1
[25] Höfer U, Breitschafter M and Umbach E 1990 *Phys. Rev. Lett.* **64** 3050
[26] Bertolo M, Hansen W and Jacobi K 1991 *Phys. Rev. Lett.* **67** 1898
[27] Gustafsson T and Plummer E W 1978 *Photoemission and the Electronic Properties of Surfaces* ed B Feuerbacher, B Fitton and R F Willis (New York: Wiley) ch 12
[28] Hoffmann R 1988 *Rev. Mod. Phys.* **60** 601
[29] Holloway S and Norskov J 1991 *Bonding at Surfaces* (Liverpool: Liverpool University Press)
[30] Rösch N 1992 *Cluster Models for Surface and Bulk Phenomena (NATO Advanced Study Institute, Series B, vol 283)* ed G Pacchioni, P S Bagus and F Parmigiani (New York: Plenum) p 251
[31] Weinelt M, Huber W, Zebisch P, Steinrück H-P, Pabst M and Rösch N 1992 *Surf. Sci.* **271** 539
[32] Ramsey M G, Steinmüller D, Netzer F P, Neuber M, Ackermann L, Lauber J and Rösch N 1992 *Surf. Sci.* **260** 163
[33] Davenport J W 1976 *Phys. Rev. Lett.* **36** 945; 1978 *J. Vac. Sci. Technol.* **15** 433
[34] Schichl A, Menzel D and Rösch N 1984 *Chem. Phys. Lett.* **105** 285
[35] Dubs R L, Smith M E and McKoy V 1988 *Phys. Rev.* B **37** 2812
[36] Nyberg G L and Richardson N V 1979 *Surf. Sci.* **85** 335
[37] Hofmann P, Horn K and Bradshaw A M 1981 *Surf. Sci.* **105** L260
[38] Braun W and Jäkisch G 1994 *BESSY Jahrbuch* (Berlin: BESSY) p 59
[39] Huber W, Steinrück H-P, Pache T and Menzel D 1989 *Surf. Sci.* **217** 103
[40] Steinrück H-P, Huber W, Pache T and Menzel D 1989 *Surf. Sci.* **218** 293
[41] Engelhardt H A, Zartner A and Menzel D 1981 *Rev. Sci. Instrum.* **52** 1161
Engelhardt H A, Bäck W, Menzel D and Liebl H 1981 *Rev. Sci. Instrum.* **52** 835
[42] Menzel D 1979 *Chemistry and Physics of Solid Surfaces* vol II, ed R Vanselov (Cleveland, OH: Chemical Rubber Company Press)
[43] Horn K, Bradshaw A M and Jacobi K 1978 *J. Vac. Sci. Technol.* **15** 575
[44] Hofmann P, Horn K and Bradshaw A M 1981 *Surf. Sci.* **105** L260
[45] Albert M R, Sneddon L G, Eberhardt W, Greuter F, Gustafsson T and Plummer E W 1982 *Surf. Sci.* **120** 19

[46] Wang L and Tysoe W T 1990 *Surf. Sci.* **236** 325
[47] Sheppard N 1988 *Ann. Rev. Phys. Chem.* **39** 589 and references therein
[48] Weinelt M, Zebisch P, Huber W, Pabst M, Birkenheuer U, Reichert B, Rösch N and Steinrück H-P 1992 *Proc. Symp. on Surface Science (La Plagne)* ed M Alnot, J J Ehrhardt, C Launois, B Mutaftschiev and M R Tempere, p 276
[49] Weinelt M, Huber W, Zebisch P, Steinrück H-P, Reichert B, Birkenheuer U and Rösch N 1992 *Phys. Rev.* B **46** 1675
[50] Stroscio J A, Bare S R and Ho W 1984 *Surf. Sci.* **148** 499
[51] Stöhr J 1992 *NEXAFS Spectroscopy* (Berlin: Springer) and references therein
[52] Turner D W, Baker C, Baker A D and Brundle C R 1970 *Molecular Photoelectron Spectroscopy* (London: Wiley)
[53] Lloyd D R, Quinn C M and Richardson N V 1977 *Solid State Commun.* **23** 141
[54] Neumann M, Mack J U, Bertel E and Netzer F P 1985 *Surf. Sci.* **155** 629
[55] Nyberg G L, Bare S R, Hofmann P, King D A and Surman M 1985 *Appl. Surf. Sci.* **22/23** 392
[56] Surman M, Bare S R, Hofmann P and King D A 1987 *Surf. Sci.* **179** 243
[57] Bertel E, Rosina G and Netzer F P 1986 *Surf. Sci.* **172** L515
[58] Mate C M and Somorjai G A 1985 *Surf. Sci.* **160** 542
[59] Othani H, Van Hove M A and Somorjai G A 1988 *J. Phys. Chem.* **92** 3974
[60] Ohtani H, Wilson R J, Chiang S and Mate C M 1988 *Phys. Rev. Lett.* **60** 2398
[61] Rauscher H, Jakob P und Menzel D 1990 *Surf. Sci.* **234** 108
[62] Jakob P und Menzel D 1990 *Surf. Sci.* **235** 15
[63] Huber W, Weinelt M, Zebisch P and Steinrück H-P 1991 *Surf. Sci.* **253** 72
[64] Steinrück H-P 1991 *Proc. Symp. on Surface Science (Obertraun)* ed P Varga and G Betz (Vienna: TU-Wien) p 67
[65] Huber W, Zebisch P, Bornemann T and Steinrück H-P 1991 *Surf. Sci.* **258** 16
[66] Heimann P A, Jakob P, Pache T, Steinrück H-P and Menzel D 1989 *Surf. Sci.* **210** 282
[67] Steinrück H-P, Heimann P A, Huber W, Jakob P, Pache T and Menzel D 1990 *J. Electron. Spectrosc. Relat. Phenom.* **52** 91
[68] Stichler M, Weimar R and Menzel D 1996 to be published
[69] Zebisch P 1995 *Doctoral Thesis* Technische Universität München
Zebisch P, Weinelt M, Trischberger P, Stichler M and Steinrück H-P 1996 in preparation
[70] Graen H H, Neuber M, Neumann M, Odörfer G and Freund H J 1990 *Europhys. Lett.* **12** 173
[71] Neuber M 1992 *Doctoral Thesis* Universität Osnabrück
[72] Netzer F P, Rangelov G, Rosina G, Saalfeld H B, Neumann M and Lloyd D R 1988 *Phys. Rev.* B **37** 10 399
[73] Schaff O, Fernandez V, Hofmann P, Schindler K-M, Theobald A, Fritzsche V, Bradshaw A M, Davis R and Woodruff D P 1996 *Surf. Sci.* **348** 89
[74] Held G, Bessent M, Titmuss S and King D A 1996 to be published
[75] Jorgensen W L and Salem L 1973 *The Organic Chemist's Book of Orbitals* (New York: Academic)
[76] Deuterated benzene (C_6D_6) has been used throughout our studies; this is of no influence on the electronic structure, but minimizes the effects of the hydrogen background signal in TPD [39, 40, 63].
[77] Fox T and Rösch N 1991 *Surf. Sci.* **256** 159
[78] Bandy B J, Chesters M A, Pemble M E, McDougall G S and Sheppard N 1984 *Surf. Sci.* **139** 87
[79] Demuth J E 1979 *Surf. Sci.* **84** 325; 1980 *Surf. Sci.* **93** 127
[80] Bao S, Schindler K-M, Hofmann P, Fritsche V, Bradshaw A M and Woodruff D P 1993 *Surf. Sci.* **291** 295
[81] Weinelt M, Huber W, Zebisch P, Steinrück H-P, Ulbricht P, Birkenheuer U, Boettger J C and Rösch N 1995 *J. Chem. Phys.* **102** 9709
[82] Freund H-J 1989 *Landolt–Börnstein New Series* vol 23a, ed A Goldmann and E E Koch (Berlin: Springer) ch 2.3
[83] Horn K, Bradshaw A M and Jacobi K 1978 *Surf. Sci.* **72** 719
[84] Horn K, Bradshaw A M, Hermann K and Batra I P 1979 *Solid State Commun.* **31** 257
[85] Batra I P, Hermann K, Bradshaw A M and Horn K 1979 *Phys. Rev.* B **20** 801
[86] Horn K, Scheffler M and Bradshaw A M 1978 *Phys. Rev. Lett.* **41** 822
[87] Weinelt M 1995 *Doctoral Thesis* Technische Universität München
[88] Weinelt M, Zebisch P and Steinrück H-P 1993 *Surf. Sci.* **287/288** 471; 1993 *Chem. Phys.* **177** 321
[89] Gallagher J W, Brion C E, Samson J A R and Langhoff P W 1988 *J. Phys. Chem. Ref. Data* **17** 9
[90] Plummer E W, Gustafsson T, Gudat W and Eastman D E 1977 *Phys. Rev.* A **15** 2339
[91] Loomba D, Wallace S, Dill D and Dehmer J L 1981 *J. Chem. Phys.* **75** 4546
[92] Sheedy J A, Gil T J, Winstead C L, Farren R E and Langhoff P W 1989 *J. Chem. Phys.* **91** 1796

[93] Dehmer J L, Parr A C and Southworth S H 1987 *Handbook on Synchrotron Radiation* vol 2, ed G V Marr (Amsterdam: North-Holland)
[94] Dehmer J L and Dill D 1975 *Phys. Rev. Lett.* **35** 213
[95] Allyn C L, Gustafsson T and Plummer E W 1977 *Chem. Phys. Lett.* **47** 127
[96] Allyn C L, Gustafsson T and Plummer E W 1978 *Solid. State Commun.* **28** 85
[97] Görling A and Rösch N 1990 *J. Chem. Phys.* **93** 5563
[98] Carlson T A, Gerard P, Krause M O, Grimm F A and Pullen B P 1987 *J. Chem. Phys.* **86** 6918
[99] Gustafsson T and Levinson H J 1981 *Chem. Phys. Lett.* **78** 28
[100] Köppel H, Cederbaum L S, Domcke W und Shaik S S 1983 *Angew. Chem.* **95** 221
[101] Köppel H, Domcke W and Cederbaum L S 1984 *Adv. Chem. Phys.* **57** 59
[102] Eiding J, Domcke W, Huber W and Steinrück H-P 1991 *Chem. Phys. Lett.* **180** 133 (erratum: 1992 **191** 203)
[103] A complete list of references is given in reference [102].
[104] Herzberg G 1966 *Molecular Spectra and Molecular Structure III* (New York: Van Nostrand Reinhold)
[105] Köppel H, Cederbaum L S and Domcke W 1988 *J. Chem. Phys.* **89** 2023
[106] Eiding J 1991 *Doctoral Thesis* Technische Universität München
[107] Bersuker I B and Polinger V Z 1989 *Vibronic Interactions in Molecules and Crystals* (Berlin: Springer)
[108] Haller E, Cederbaum L S and Domcke W 1980 *Mol. Phys.* **41** 1291